Evaluation of Alternate Bearing Designs in a High Speed Automotive Turbocharger

Brian David Mondschein

Thesis submitted to the faculty of the Virginia Polytechnic Institute and State University

in partial fulfillment of the requirements for the degree of

MASTER OF SCIENCE

in

MECHANICAL ENGINEERING

Gordon Kirk, Chairman

Walter O-Brien, Member

Robert West, Member

June 9, 2010

Blacksburg, Virginia

Keywords: Turbocharger, Stability, Bearing, Design

Evaluation of Alternate Bearing Designs in a High Speed Automotive Turbocharger

Brian Mondschein

ABSTRACT

Automotive turbochargers experience self-excited instabilities through the majority of their operating speed range. The results of these instabilities can cause damage to the bearings, shafts, and housing walls. Preventing this damage while maintaining or increasing performance characteristics is a huge concern to industry due to the time and money needed to replace vital components.

The aim of this research is to determine which characteristics of the bearings have the greatest influence on the damped natural frequencies. It was believed that axial groove bearings could offer an acceptable alternative to the floating ring bearings currently found in automotive turbochargers. DyRoBeS rotor dynamics software was used to determine analytically damped natural frequencies for floating ring bearings, and also for six, eight, and ten axial groove fixed geometry bearings, under different speed and loading conditions. The resulting data were compared to experimental test results from an on-engine turbocharger test stand and presented in this report.

Acknowledgements

There are so many people that deserve recognition for keeping me on the right track in pursuit of academic progress. First and foremost Dr. Kirk, my graduate advisor. Not only has his passion for rotor dynamics been a very positive influence in my academic career, but his impeccable ability to work around my seemingly impossible schedule is the sole reason I was able to even begin this challenge. Along the same lines, I would like to thank Cathy Hill, who will never receive the recognition she deserves. Her constant work to keep all of the t's crossed and i's dotted along my path was no small feat.

A special thank you to my parents, who have taught me that hard work overcomes all frustration. The never ending love, support (both emotional and financial), and positive influence have kept me going through so many trying times. Despite my best efforts, I don't know that I will ever be able to thank you for all that you have done for me. Also thank you my brother Stephen, who constantly challenged me by trying to finish first.

Thank you to the faculty and staff of the Mechanical Engineering department at Virginia Tech. Throughout both my undergraduate, and graduate career, I have been thoroughly influenced by their level of dedication and encouragement. Wherever I may go, I will certainly try to represent this university to the best of my abilities.

And finally, huge thanks to Dr. Robert Phillips, my coach and mentor. To whom I will be forever indebted. His guidance and advice has been vital in my development as not only an athlete, but as a student, and a person. He, and the rest of my pole vault family, was a source enjoyment in every outside of the classroom.

Dedication

This paper is dedicated to the loving memory of my best friend and brother in life Timothy Husted. I will always cherish the great times we shared growing up. Late nights in the garage working on cars, or sunny days on the Delaware shore. I miss you everyday my friend.

Table of Contents

List of Figures

List of Tables

Nomenclature

PSI – pounds per square inch

FR Bearing, FR – Floating Ring Bearing

6AG – 6 axial groove bearing

8AG – 8 axial groove bearing

10AG – 10 axial groove bearing

DNF – damped natural frequency

DyRoBeS– Dynamic Rotor Bearing Software

FR-FR – FR on compressor side, FR on turbine side

6AG-FR – 6AG bearing on compressor, FR on turbine side

8AG-FR – 8AG bearing on compressor, FR on turbine side

10AG-FR – 10AG bearing on compressor, FR on turbine side

RPM – Revolutions per minute

CPM – Cycles per minute

FEA – Finite Element Analysis

CHAPTER 1

Introduction and Literature Review

1.1 Introduction

Turbochargers were first developed in 1885 as a means to increase the thermodynamic efficiency of diesel engines [1]. This was accomplished by means of an exhaust driven compressor wheel force feeding additional air, more importantly oxygen, into the engine, allowing more fuel for combustion.

While first used in aircraft around 1915, the use of turbochargers for automobiles began to appear in the late 1930's [1]. Today turbocharged gasoline motors have produced some of the most powerful street cars in existence. Motors such as the Toyota code 2JZ-GTE have produced over 700hp with only 3.0 liters displacement. Despite their popularity in the racing world, the most widespread application of the turbocharger is found on diesel engines, both industrial, such as generators and bulldozers, and commercial passenger vehicles.

Centrifugal turbochargers (such as those found in both gasoline and diesel powered automotive vehicles) are composed of a surprisingly low number of main components. There are essentially two separate housings which enclose two fan blade wheels connected by a rotating shaft [2]. These shafts are typically run through floating ring bearings which allow them to spin freely. Additionally, most turbochargers use a wastegate (a pressure regulated valve) to maintain proper boost levels. Figure 1.1 shows the basic assembly of a turbocharger shaft including the bearings and wheels.

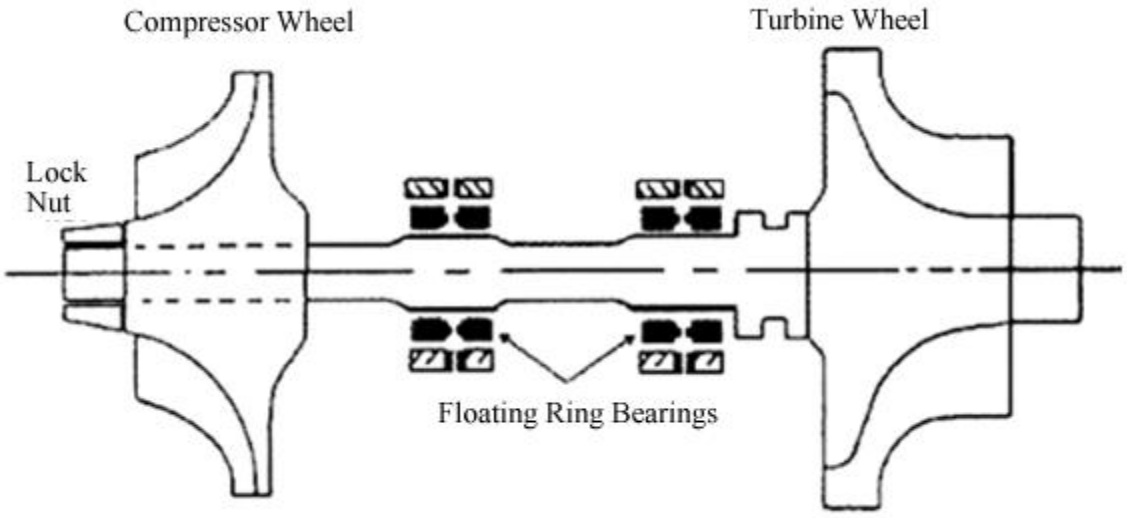

Figure 1.1.1: Parts diagram of automotive turbocharger

The compressor wheel is usually made of aluminum (either LM-16 WP or C355T61), as is the compressor housing (LM-27). Because the turbine experiences higher temperatures, aluminum can not be used and the blades are typically made from Inconel, which can withstand the required 1340^{o}F. The turbine housing can either be made from spheroidal graphite cast iron, for lower temperature requirements, or nickel cast iron for higher operating temperature requirements. A high carbon steel (C1144) is used for the turbocharger shaft because it can withstand the high stresses of operation, and allows induction hardening of the journals [3].

Axial turbochargers may be made up of one or more stages. Aircraft turbojet engines contain multiple axial stages. The compression ratio is one measure of performance for a compressor, and is defined as the ratio of absolute discharge pressure to absolute intake pressure. When the compression ratio is too high for a given stage, high discharge temperature and design problems occur. Instead of a single stage, multiple

stages are used to allow a more gradual increase in pressure. An example of a multistage axial compressor is found in Figure 1.2

Figure 1.1.2: Multistage Axial Compressor

Basic thermodynamics of turbochargers is relatively simple. Hot exhaust gases expelled from the engine, which otherwise would go to waste, spin the turbine wheel located on one side of the shaft. This, in turn, spins a compressor wheel located on the intake side of the engine [4]. The compressor wheel draws in and "compresses" the air, typically to 10-30 psi for automotive diesel applications. Depending on the level of additional air forced into the engine, the fuel system will supply a corresponding amount of extra fuel to balance combustion stoichiometrically. This process is represented by Figure 1.1.3.

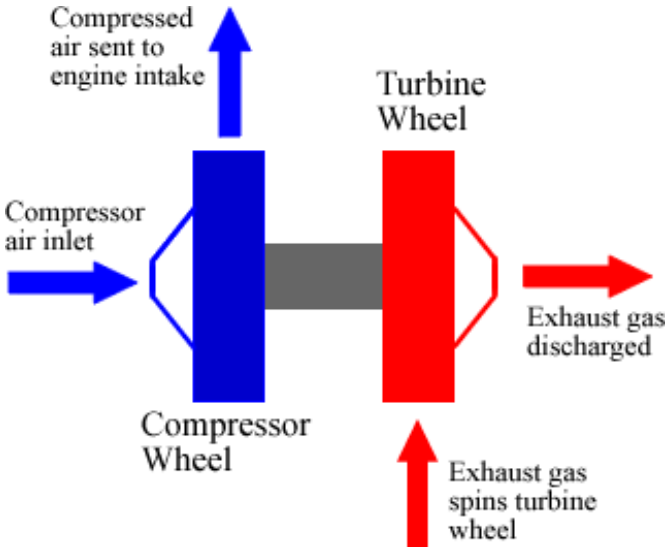

Figure 1.1.3: Turbocharger air flow diagram

Additional gains can be accomplished by cooling the compressed air before it reaches the motor. This is accomplished using an air-air heat exchanger, known as an intercooler, which makes use of ambient air to dissipate heat into the surroundings. With the added fuel, typical power gains for automotive applications range from 30-40 percent.

As with most performance driven products, there is a significant level of compromise among cost, reliability, and performance. This is especially true in turbochargers, which frequently see speeds above 100,000 RPM. As the bearings, seals, and o-rings begin to wear, the connecting shaft is subjected to ever-changing levels of vibration and imbalance. If the amplitude of these vibrations and imbalance become too large, the turbocharger can suffer from sudden catastrophic failure ranging from spun bearings to fragmented blades. Also, contamination in the oil or oiling system can result in oil pressure insufficient for these high-speed parts to run freely and smoothly. Dry running of the turbocharger quickly leads to bearing failure. In some cases, pieces of the failed turbocharger may pass into the motor, resulting in destruction of internal components including pistons or cylinder walls. In the case of turbocharged power plants,

results of such failure can cost millions of dollars in lost time and equipment. Even simple maintenance of large scale turbochargers can cost millions in lost time and productivity.

Reliable bearings are essential to reliable turbocharger operation. Turbocharger shafts are known to experience self-excited vibration, which adds additional stress and instability to the turbocharger shaft. Over time, stress causes wear on the bearings, allowing the shaft to spin outside of its intended operating region leading to failure of the turbocharger. Another method of failure is acute overload. In the event of a large self-excited instability, or pressure regulation failure, including failure of the wastegate, the bearings become overloaded and can strike the walls of the housing.

The present research focuses on testing three custom bearings, featuring axial grooves, to reduce instabilities without loss of performance. Experimental turbocharging vibration results were available from the Virginia Tech Rotor Lab. The results were used for calibration of a DyRoBeS analytical model. The calibrated model was used to perform a stability analysis under a variety of speed and load conditions.

1.2 Literature Review

Lateral vibration response of turbochargers can be categorized as either self-excited or a result of unbalance. Unbalance occurs in rotor bearing systems because of two principle causes. Mass eccentricity is a natural phenomenon due to an offset in the center of mass. Shaft bow is due to the thermal effects. These unbalance vibrations are synchronous with shaft speed and can be solved by balancing the rotor or re-straightening the rotor shaft [5].

Self-excited vibrations only develop during the operation of the turbocharger. When the turbocharger stops, the self-excited vibrations disappear. Instabilities can occur at the damped natural frequencies and usually below running speed. Causes for self-excited vibrations can be whipping and whirling, parametric instabilities, stick-slip rubs and chatter, and instabilities in forced vibrations [6]. This research focuses on whipping and whirling instabilities. Whipping and whirling are the subsynchronous instabilities of turbochargers. The main sources of these are internal damping, and aerodynamic cross-coupling.

Past studies of rotor dynamic analysis have been scarce due to the high expense and difficulty. Dr. Tanaka used a modified Reynolds equation to perform analytical calculations on the fluid films. It was determined the inner fluid film plays a greatly more significant role in stability than does the outer film for a floating ring bearing [7]. In 2005, a design team of senior engineering students at Virginia Tech began development of an on engine test stand for the purposes of stability analysis. A combination of custom designed parts and stock components were assembled in the dynamometer area in Randolph hall [3]. Preliminary testing performed in the spring of 2006 showed that the designed test stand was able to identify two expected unstable mode frequencies for the stock floating ring bearing. Data collection procedures were established and made for easy documentation and understanding of the test results [8].

A full study on the influence of adding unbalance in an effort to balance the rotor and minimize subsynchronous unbalance instabilities was performed on the test stand by John Sterling in 2009. It was determined that the addition of unbalance on the compressor wheel can suppress these vibrations. Further studies were recommended to determine the

amount of unbalance to leave on the rotor because balancing the rotor completely is not practical for field operation [9].

Recent developments in finite element software have made analytical study easier, faster, cheaper, and more accurate. In 2005, Dr. Ali Alsaeed, Virginia Tech PhD, documented a purely analytical study of bearing instability in an automotive turbocharger using Dynamic Rotor Bearing Software, DyRoBeS. His model successfully calculated first and second mode instabilities, and performed a transient analysis. It was determined that FR bearings, while operating at a turbocharger speed of 100,000RPM, exhibit self-excited instabilities at 10k and 23k cpm [6]. At the time there was no experimental data for comparison so the dependability of his model for predicting damped natural frequency content was not known.

Bearing fatigue failure prevention is largely dependant on the oil lubrication system. Floating ring bearings, known as sleeve bearings, surround the turbocharger shaft and allow it to spin freely by means of an oil film layer. The layer of oil not only acts as lubrication and heat dissipation, but also serves as a damper to improve the stability of the system. One oil film is located between the shaft and the inner diameter of the bearing. A second film is located between the housing and the outer diameter of the bearing.

Because of its damping function, the thickness of the oil layer has a large effect on the shaft stability so the clearances of the bearing-shaft system need to be considered thoroughly when designing the bearing. Floating ring bearings can be classified by their relative length compared to the radius of the bearing. For a long bearing the length, L is much greater than the bearing radius, R (L>>R) [10]. A short bearing, found in

automotive turbochargers, has L less than the bearing diameter. A finite length bearing has L approximately equal to R. The analysis of loads and instabilities changes with bearing type.

A draw back to fluid film bearings is their inability to support load when whirling at half shaft speed [10]. Special design profiles must be created to redistribute fluid pressure around the bearing. A second drawback to the fluid film bearing is the high dependency on the lubricating fluid. The oil system is shared with the engine system for cost efficiency [2]. Contamination in the common fluid can cause undesirable heat levels in the bearings and shaft. In the event of oiling failure anywhere in the system, sudden, catastrophic dry-running of the turbocharger can occur, leading to instantaneous failure. Axial grooves may improve the oil circulation and help prevent premature failure. These grooves are machined in various patterns on the inner surface where the turbocharger shaft passes through. Custom bearings have been manufactured with six, eight, and ten grooves in the inner wall, parallel to the turbocharger shaft.

Previous bearing studies confirm that altering the bearings can greatly affect rotor-dynamic stability. In 2003, Dr. Pettinato experimentally documented the affects of modifying oil flow in thrust bearings on turbocharger performance. Results showed that increasing oil flow, through the use of lobes, decreased the amount of forces on the bearing and resulted in lowering operating temperatures by roughly 20 percent and reducing self-excited instabilities [11].

One of the current new technologies improving turbocharger performance is the use of variable geometry. Turbochargers often suffer from a condition known as “turbo lag”. “Lag” is caused by the lack of exhaust flow at low engine speeds, resulting in the

inability to spin the compressor wheel. Without this compression, there is no additional power created by the turbo at low engine speed. By using configurable geometry at either the turbine or compressor side of the turbocharger, the input flow angle therefore air flow rate, can be altered.

Variable geometry makes use of adjustable guide vanes at the inlet of the compressor wheel. When the vanes are closed additional load is created on the turbine side, which allows the turbo to reach higher speeds even when the engine is at low RPM. As the engine speed increases, the vanes can open allowing the turbo to reach its full flow rate and maximum power. Because most turbochargers implemented in production vehicles are designed to be a compromise of between lower RPM power and top end power, these variable geometry turbochargers allow the creation of more power through the RPM band, and a higher peak horsepower.

Both Borg Warner and Holset have done developmental work on variable geometry turbines and have found these to provide a wide variety of benefits. Increased fuel efficiency and improved exhaust gas recycling are two of the benefits to this design. Also because of the increased power efficiency, a smaller turbocharger can now output the same amount of power which reduces both volume and weight taken up by the turbocharger.

Another technology that is actually making a returning to implementation in turbochargers is the use of air bearings. While not new, recent developments have brought air bearings back into consideration for replacing the floating bushing bearings commonly found in modern turbochargers. Air bearings, also known as bump foil bearings, are a style of bearing designed to use a layer of air, rather than oil, to keep the

shaft spinning smoothly. The two main components to an air bearing are the top foil and the bump foil.

The shape of the bump foil layer is designed to pump air between the moving surfaces creating pressure. This pressure acts much like automotive shock absorbers, using a cushion of air to support the vehicle. On of the greatest benefits to this is the faster the turbocharger spins, the more air pressure is created. This increased air pressure gives the shaft greater support at higher speeds. Air bearings have less scheduled maintenance caused by the lack of necessity for an oiling system. In the event of failure, the foils restrain the shaft from moving, confining damage to the shaft and bearing, and protecting the housings [12].

Air bearings have actually been in production for a number of years, commonly used in computer magnetic drives. Turbocharger use is more difficult to implement due to problems with low speed operation. At low speeds the air bearing actually touches the turbocharger shaft. The wear caused by the bearing-shaft contact led to problems because a suitable coating for the turbocharger shaft could not be found that both protected it from the high temperatures experienced by the turbocharger (800-900 ºF) and did not wear at low speeds. Due to this issue, bump foil bearings were limited to applications which remained below 400 ºF [12].

Ball bearings are not commonly used in commercial vehicles due to short lifespan and difficulty replacing components. High performance engines for racing applications sometimes make use of ball bearing turbochargers as a result of decreased operating times and increased budget. These are usually made of more expensive ceramic ball bearings in place of steel. [2]

Chapter 2

Testing Equipment

2.1 Rotor Bearing Software for Analytical Data Acquisition

Two programs, developed by Wen Jen Chen, Ph.D, were used for analytical data generation. DyRoBeS (Dynamic Rotor Bearing Software) Rotor is a rotor bearing analysis tool that uses the Finite Element method to perform lateral, torsional, and axial vibration analysis [13]. The DyRoBeS rotor program is capable of performing critical speed analysis, whirl speed and stability analysis, steady state response, and time transient analysis both linearly and nonlinearly. This research will focus on linear whirl speed and stability analysis.

DyRoBeS BePerf is a program developed to analyze the bearing steady state and dynamic performance. Various bearing types can be modeled and studied including fixed lobe bearings, tilting pad bearings, and floating ring bearings. Analysis can be performed under constant viscosity assumptions, or with varying viscosity under calculated temperatures [6, 14]. Final work was done on fixed lobe and floating ring bearings under the constant viscosity assumption.

The rotor was modeled by Dr. Alsaeed, in coordination with the manufacturer, through previous research done at Virginia Tech. Using DyRoBeS Rotor, the turbine and shaft were created as a single jointed body. The aluminum compressor wheel was assumed as added disks to the rotor [6]. The bearings were modeled as specified by the manufacturer. Two materials were used in the DyRoBeS model of the stock turbocharger. The rotor shaft is made of carbon steel and the turbine wheel of Inconel. Unbalances were also entered as specified by the manufacturer. The nominal diameter of the shaft is 0.433

inches. The total length of the turbocharger is 6.244 inches and has a mass of .8941 lbs. The polar inertia of the compressor wheel increased from left to right to match the changing profile of the wheel. The inertia values began and .000172 in^4 and increased to .00399 in^4 at the largest point on the wheel. On the turbine end, the values decreased from .0080 in^4 to .00030 in^4 also to represent the changing profile of the turbine wheel.

DyRoBeS BePerf was used in modeling the stock and custom bearings. The FR diameter is .626 inches and has a mass of .017lbs. The nominal length of the bearing is .267 inches. DyRoBeS only allows the floating ring bearings to be run as constant viscosity. The inner and outer film viscosities were input as $4.93e^{-7}$ Reynolds on the turbine bearing, and $1.12e^{-6}$ on the compressor end. The 6, 8, and 10AG bearings were defined as fixed geometry bearings with a density of 0.24 lbm/in^3, and a length of .267 in. Viscosity was set at 1.12e-6 Reynolds for the constant viscosity solver. The heat balance solver was not used in this analysis. DyRoBeS BePerf does not allow computation of FR bearings with heat balance. Also, even under light loading, the heat balance solver struggled to converge a solution. Further details of both the turbocharger and bearings are proprietary information and can not be disclosed as per the original agreement with the manufacturer.

Unloaded cases were performed with the only gravity loads applied to the wheels. On the compressor end 0.1lbs of loading was set, along with 1.0lbs on the turbine end. The lateral analysis was performed for whirl speed and stability. The stiffness were determined as an average of the x and y stiffness. The starting speed and ending speeds were set at 25k and 150k respectively. For this analysis, it was selected that DyRoBeS would return the first 6 modes. No other options needed to be set for this type of analysis.

A screen capture of the BePerf software is provided in Figure 2.1.1 and a screen capture showing Rotor software running the stock turbocharger model is provided in Figure 2.1.2.

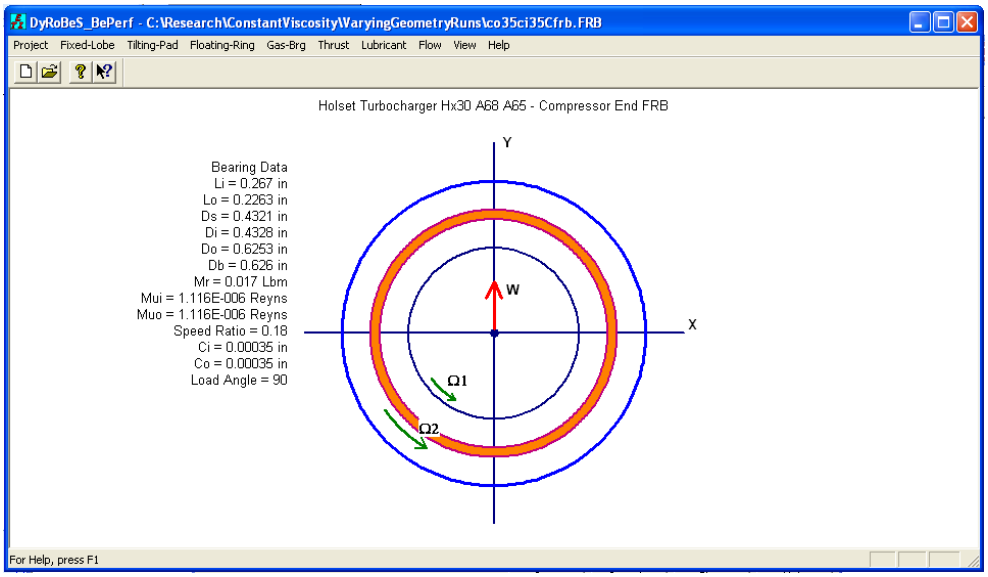

Figure 2.1.1 User interface of DyRoBeS BePerf Software

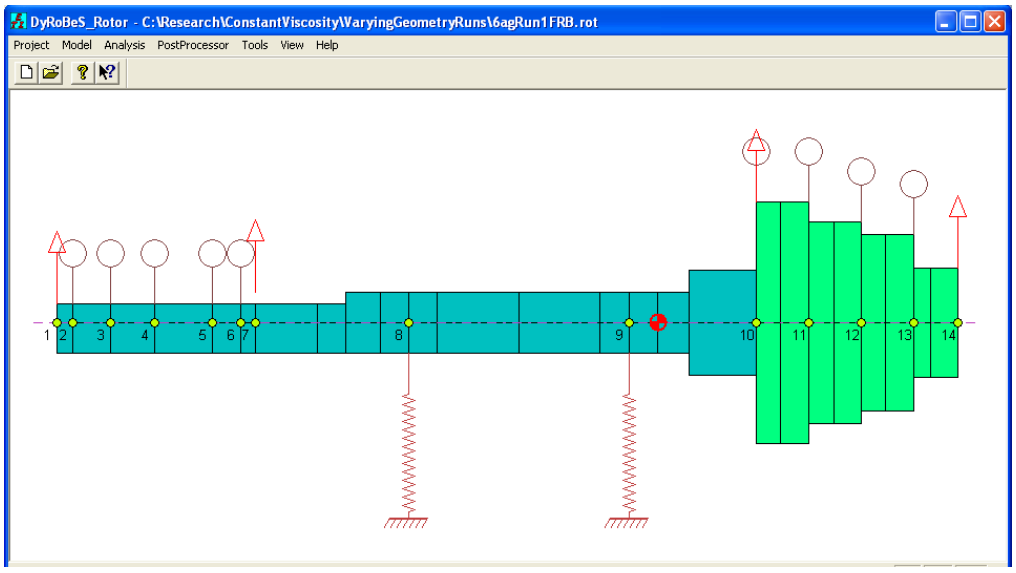

Figure 2.1.2: User interface for DyRoBeS Rotor software

2.2 Engine and Turbocharger for Experimental Data Acquisition

For data collection, a test stand designed by a senior design team at Virginia Tech in 2006 was used [3]. A Cummins 4BT 3.9 liter diesel engine was installed on a cast iron base. The testing room has the required fuel, exhaust, coolant lines, and electrical lines. The engine has the option to be mated to a dynamometer with variable loading capability. The Cummins 3.9 liter engine is typically industrial, construction, and agricultural applications. It produces 130hp and 255 ft-lbs of torque. The Cummins engine is an inline four cylinder engine with a bore and stroke of 4.02 inches and 4.72 inches and has a wet weight of approximately 750 pounds. During experimental testing, the engine was run with 15W40 oil as was specified by Cummins.

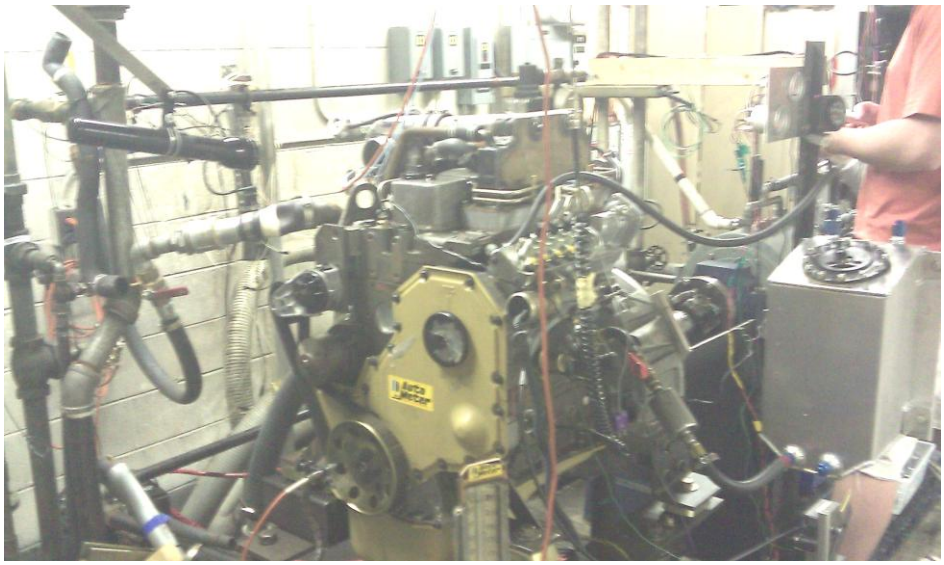

Figure 2.2.1: Experimental engine and turbocharger set up

The stock turbocharger was modified for stability studies on the developed test stand [8,15]. The turbo is capable of providing an additional 90-240 hp to engines up to 5.0 liters in size. Both the turbine wheel and compressor wheel each measure 70mm in

diameter. Air flow rates up to 7.7 pounds per second may be accomplished and regulated via wastegate system.

The stock turbo includes floating ring bearings on both the compressor and turbine sides of the turbocharger. Additionally the design team interchanged the compressor bearing with 6AG, 8AG, and 10AG versions.

2.3 Instrumentation for Experimental Data Acquisition

Instrumentation for the test stand was developed by the student team in 2006. A key piece of instrumentation is the optical speed sensor, which measures the rotational speed of the compressor wheel at the inlet. The speed sensor requires adequate lighting and a clearly distinguishable reference point for the completion of one revolution. Required lighting was originally provided by mounting a basic flashlight on a studio microphone stand which could be repositioned easily. High levels of vibration caused by the running engine necessitated a new lighting system isolated from the floor. A new ceiling mounted system was implemented, as shown in Figure 2.3.1, to prevent the engine vibrations from affecting the lighting. To distinguish a single revolution, a single blade, known as the keyphasor blade, was painted with a coat of highly reflective white paint. The rest of the blades were painted flat black paint to reduce risk of accidental pick up. The keyphasor blade can be seen in Figure 2.3.2.

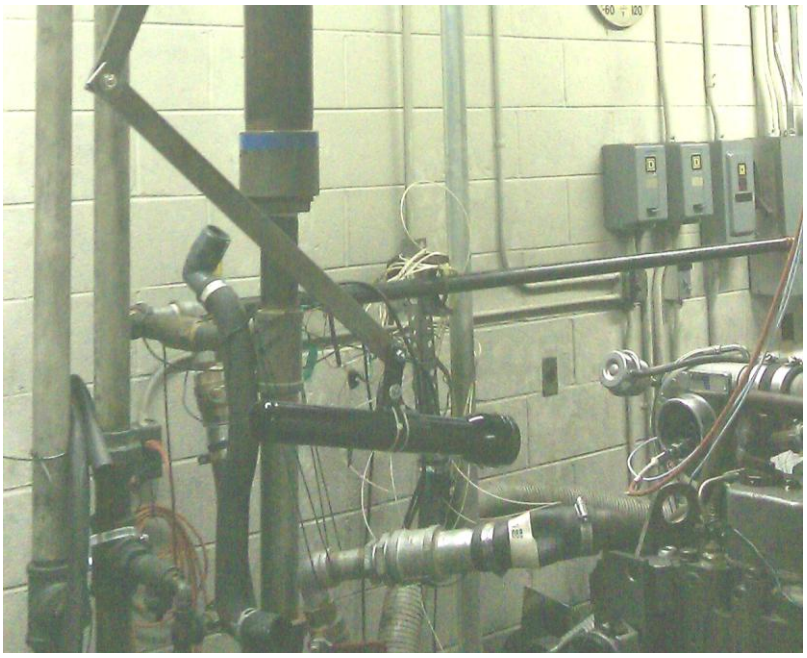

Figure 2.3.1: Ceiling mount for speed sensor light source

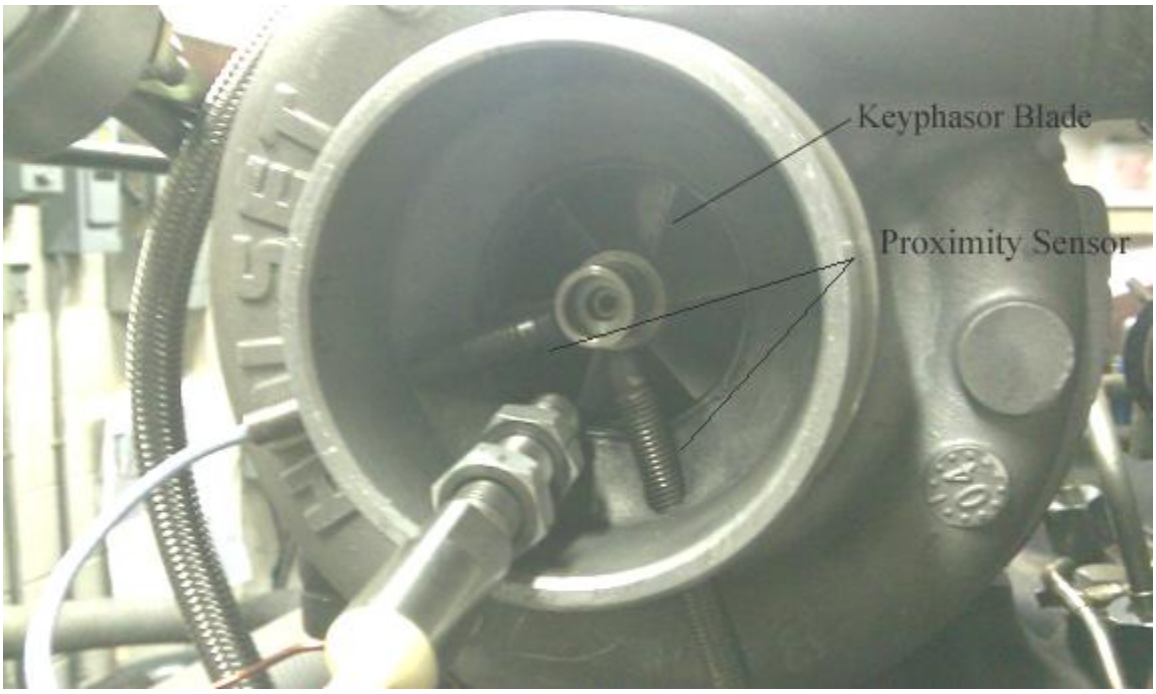

Figure 2.3.2: Close up of keyphasor blade used for speed sensor

A non-contact system of turbocharger shaft vibration measurement was accomplished using a target nut on the compressor end of the shaft. Two orthogonally installed Bently Nevada proximity sensors were used in conjunction with the target nut to provide motion tracking of the shaft end in both x and y directions. A non-contact system of measurement was needed to prevent interfering with the vibration results. The proximity sensors can be seen in Figure 2.3.2, above.

The data from the speed sensors and proximity probes was output to a data acquisition cart composed of:

- 8 channel ADRE P-208 DAQ system
- 2xy oscilloscopes
- Keyphasor signal conditioner
- Bentley Nevada amplitude, phase, and speed vector filters
- Dynamometer speed control.
- Power supplies

Figure 2.3.3: Data acquisition cart

Basic engine parameters were monitored in real time using a simple gauge cluster mounted inside the test stand room. These included Autometer oil pressure, turbocharger boost pressure, and water temperature gauges.

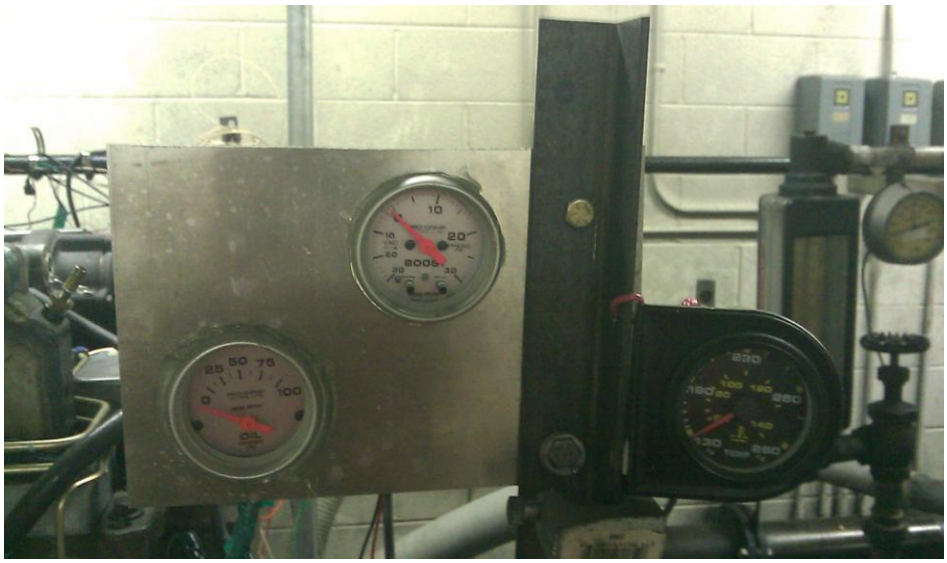

Figure 2.3.4: Gauge panel displaying engine vitals

CHAPTER 3

Procedure

3.1 Experimental Procedure

Experimental data for the instability characteristics of the various bearing types were recorded by the 2010 senior design turbocharger team. All testing was done with FR bearings mounted on the turbine side of the turbocharger shaft. Experimental data were gathered after interchanging FR, 6AG, 8AG, and 10AG bearings on the compressor side of the turbocharger shaft.

A loading procedure was developed by the research team in 2006. The engine idled until the coolant temperature increased to190^{o}F [3]. The engine speed was slowly increased to allow the data acquisition system to properly retrieve the data. The engine accelerated to a maximum speed of 2800 RPM and then loaded. This loading reduced the speed to 2500 [3]. Turbocharger speeds for the 6AG and FR bearings achieved speeds over 140k RPM. The stock experimental turbocharger is capable of an operating speed of near 150k RPM. The data acquisition software generated the cascade plots that were used to select the damped natural frequencies.

3.2 Analytical Procedure

A linear analysis of the turbocharger under various speeds and loading conditions was performed for each of the different bearing types using DyRoBeS Rotor software. Before this simulation was run, each of the bearings was modeled and analyzed using the BePerf software.

The four types of bearings used in the experimental analysis were supplied with blueprints which served as the basis of the geometric modeling. Experimentally, however, there is no method of determining the temperatures experienced inside of the housings for both the turbine and compressor ends of the turbocharger. Therefore expansion of the material could not be known, and the exact geometry could not be calculated.

The ultimate goal of these models was to be able to predict analytically the stability characteristics without the blind risk of damage to the motor or turbocharger by experimental testing, it was important to calibrate the software model to match the experimental data acquired by the turbocharger team. For the initial geometric estimates, gravity loads were applied to the compressor and turbine wheels through the BePerf software. The weight difference, in both magnitude and direction, of the turbine wheel compared to the compressor wheel, made it important to recognize that the bearing loading is different even for the same bearing on both ends. The FR bearing on the compressor side differed from the FR bearing on the turbine side, and therefore was modeled accordingly.

Bearing analysis was performed for speeds from 25k RPM through 150k RPM in 25k RPM increments. For each speed, the eccentricity of the bearing was calculated. Should the eccentricity reach 1.0, it would indicate the bearing had come in contact with the housing wall, potentially damaging the turbocharger. In addition the BePerf program output a bearing file which included the stiffness and damping characteristics of the bearing at each speed increment.

Using the DyRoBeS model, the bearing characteristics were uploaded into the DyRoBeS Rotor program for both the compressor and turbine ends. A lateral stability analysis was then run. Paralleling the experimental tests, the analytical runs were performed with the FR BEARINGS on the turbine end for all runs while the compressor end was exchanged among the FR, 6AG, 8AG, and 10AG bearings. The results of the lateral analysis provided log decrement and mode shape for each of the damped natural frequencies. A negative log decrement value represented an unstable damped natural frequency.

The 1st and 2nd unstable modes calculated were compared to the experimental cascade plots generated by the turbocharger team. Unfortunately, with the bearing geometries originally selected, the damped natural frequencies for the unstable modes were inaccurate when compared to the experimental frequencies. The bearings were remodeled, and the lateral analysis was then run again. Each time the analysis was run, the new analytical results were compared to the experimental results until the first mode values closely matched. The exact frequencies for both experimental and analytical will be discussed in the results section.

Once the final bearing geometries were determined, all of the cases were rerun with the unstable mode frequencies and mode shapes recorded. Previous work suggests that modeling the turbocharger load on the compressor wheel rather than the turbine wheel is more representative of actually operation characteristic [6]. Therefore the FR and 6AG cases were run applying 5, 10, 15, 20, and 25 pound loads force on the compressor. To mimic the loading on the compressor wheel, the equivalent loads experienced by each of the bearings were statically determined and input into DyRoBeS bearing performance.

The stiffness and damping characteristics were then calculated and exported to be used in the Rotor software in the same manner as the unloaded cases. The goal was to run each bearing with as much load as DyRoBeS could handle. Beginning with 5 lbs and increasing 5lbs at a time, the loading was applied until DyRoBeS could no longer converge a solution. Coincidentally, the maximum loadings for the 6AG and 8AG were multiples of 5. The 6AG, 8AG, 10AG bearings could hold 25, 15, and 1.5 lbs of load respectively. The loads were calculated by statically balancing the loads based on shaft lengths and bearing span. The hand calculated bearing loads are summarized in Table 3.2.1. Figure 3.2.1 shows the loading diagram for the bearings as a result of compressor loading,

Table 3.2.1: Equivalent Bearing Loads

Compressor Load (lbs)	Compressor Bearing Load (lbs) @90 degrees	Turbine Bearing load (lbs) @270 degrees
5	2.9	3.2
10	5.6	5.5
15	8.1	7.6
20	11.1	10.0
25	14.1	12.0

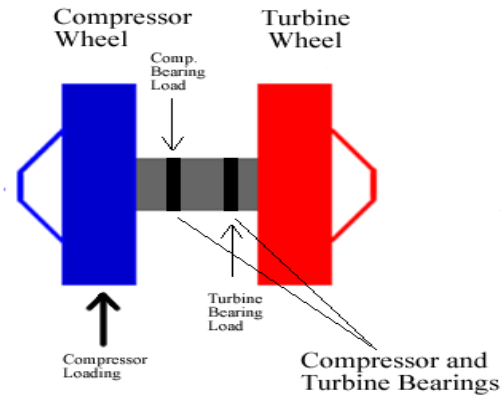

Figure 3.2.1 Resultant bearing forces due to compressor loading

CHAPTER 4

Results and Conclusions

4.1 Experimental Testing Results

The undergraduate turbocharger team recorded data for unloaded test runs using all four bearing types on the compressor end. The floating ring bearing exhibited two self-excited modes present through the operating range. Waterfall plots show a variety of frequency content. The x-axis represents the actual frequency, the left y axis is time, and the right y axis is the Keyphasor frequency which is equal to 1/3 the actual running speed. The frequency content explanation is shown on Figure 4.1.1 from the waterfall plot shown in Figure 4.1.1 the first mode frequency was located at 20,000 cpm and the second mode at 35,000 cpm. These results are shown in Figure 4.1.1.

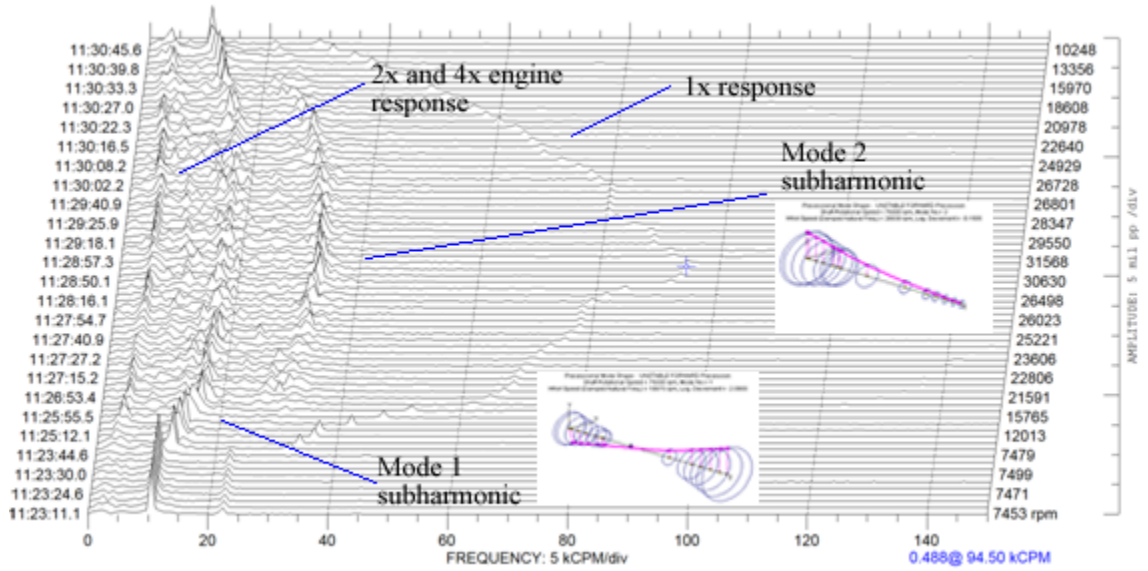

Figure 4.1.1: Waterfall plot for unloaded FR compressor bearing showing engine 2x, 4x, and turbo 1st and 2nd mode

The 6AG bearing also showed two self-excited modes throughout the operating speed range. The first mode and second modes dropped to 15,000 cpm and 26,000 cpm, respectively. The results of the 6AG test run, shown in Figure 4.1.2, show damped natural frequency values well below those of the FR bearing. The 8AG and 10AG decreased further from even the 6AG results. The first mode damped natural frequencies dropped to 12,000 cpm and 10,000 for the 8AG and 10AG, respectively. The second modes were too washed out to be determined from the waterfall plots. The results from these runs are shown Figures 4.1.3, and 4.1.4. A summary of the damped natural frequencies for all bearings being is displayed in Table 4.1.1.

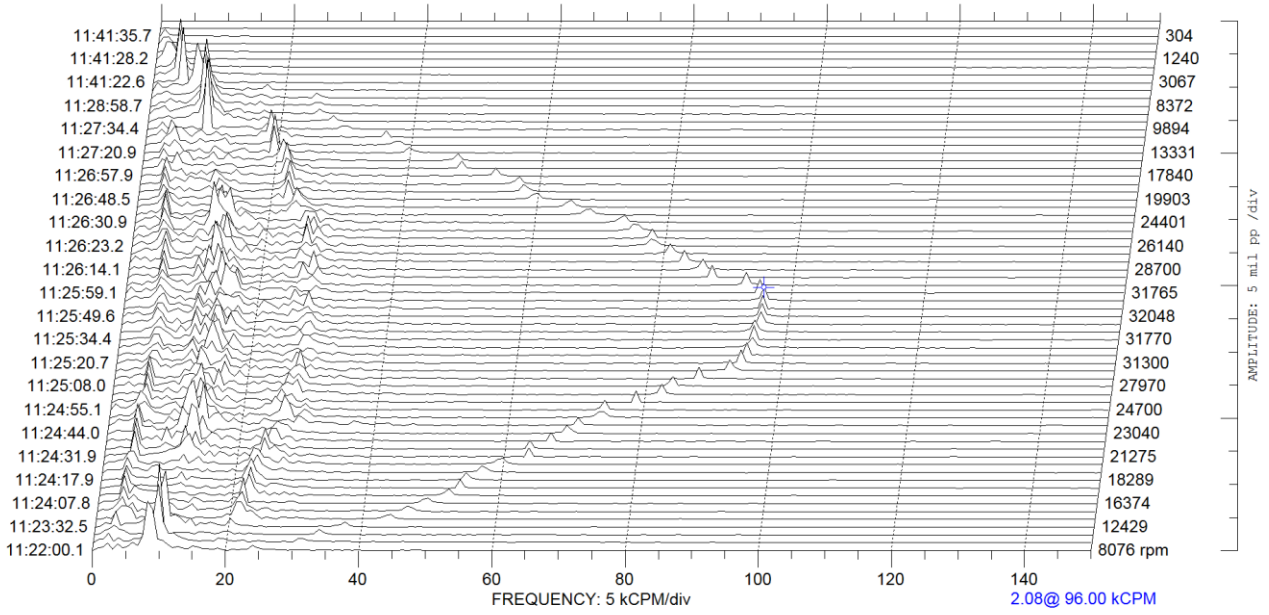

Figure 4.1.2: Waterfall plot for unloaded 6AG compressor bearing showing engine 2x, 4x, and turbo 1st and 2nd mode instability

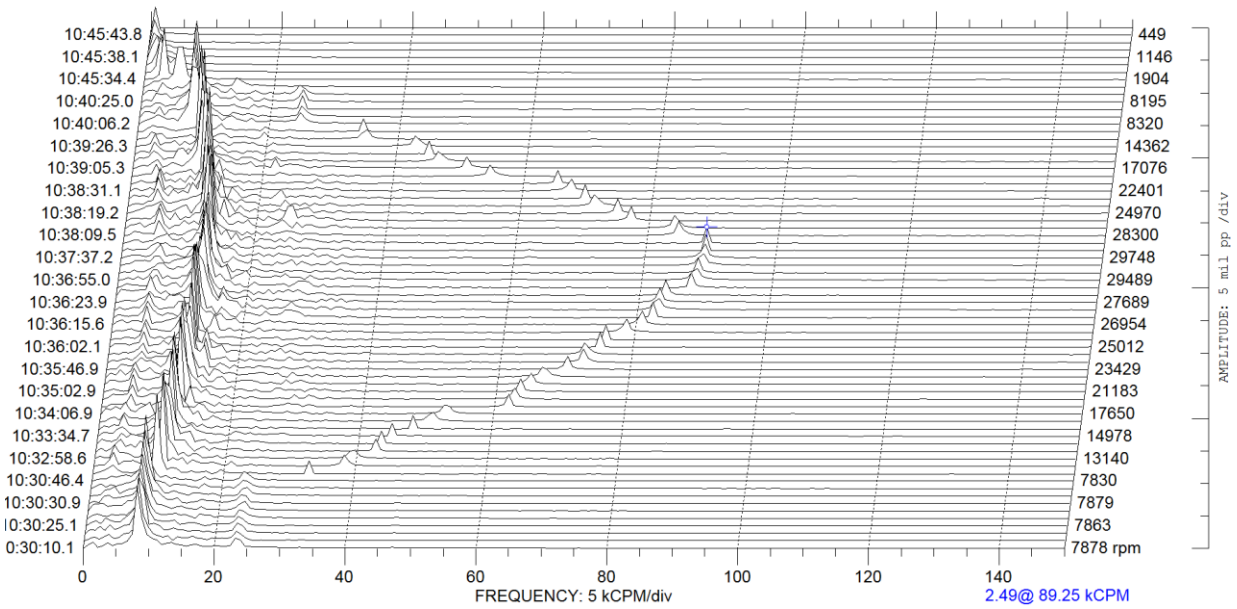

Figure 4.1.3: Waterfall plot for unloaded 8AG compressor bearing showing engine 2x, 4x, and turbo 1st mode instability

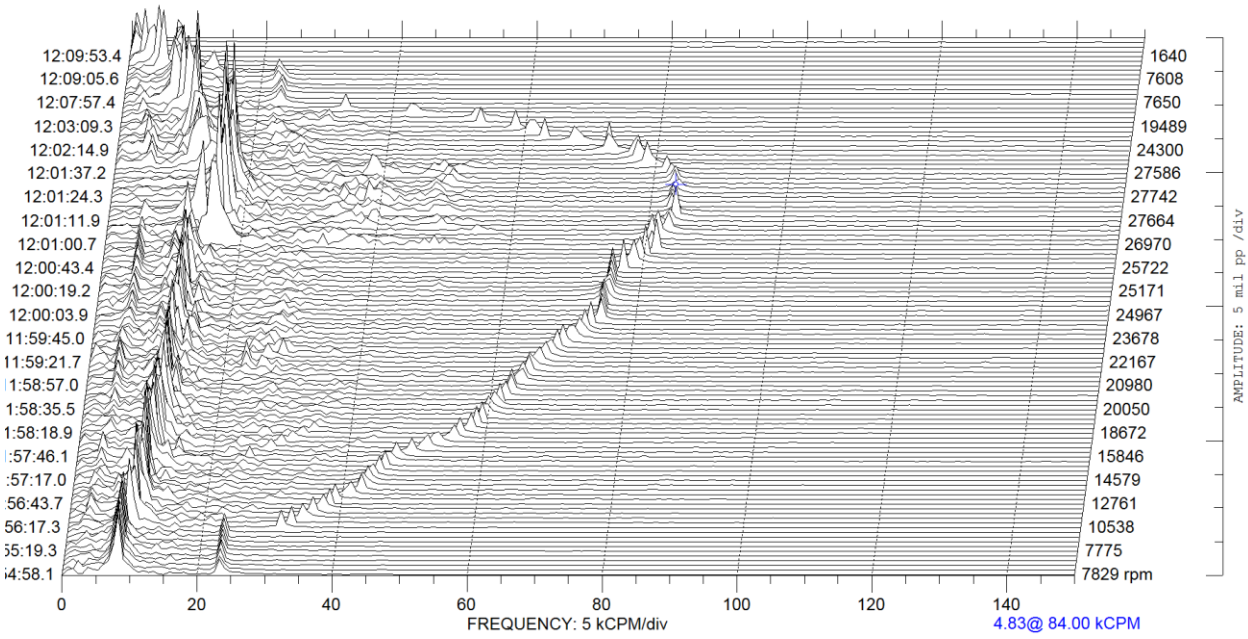

Figure 4.1.4: Waterfall plot for unloaded 10AG compressor bearing showing engine 2x, 4x, and turbo 1st mode instability

Table 4.1.1 – Comparison of damped natural frequency for each bearing type

Bearing on Compressor	Mode 1 Frequency (cpm)	Mode 2 Frequency (cpm)	Max Turbocharger speed (cpm)
Floating Ring	20,000	35,000	97,200
6AG	15,000	26,000	96,000
8AG	12,000	Not distinguishable	89,250
10AG	10,000	Not distinguishable	84,000

4.2 Influence of Bearing Clearances on Damped Natural Frequencies

The FR, 6AG, 8AG, and 10AG bearing cases run by the undergraduate research team became the baseline calibrations for the analytical bearing models. The high operating temperatures experienced by the bearings and shaft cause thermal expansion making the precise inner and outer bushing clearances difficult to determine. A first approximation was calculated based on the thermal expansion coefficients of the various components. A sample of the results of these calculations is found in Figure 4.2.1. The full calculations are found in Appendix A.

Based on the thermodynamic calculations, the inner diametric clearance for both the turbine and compressor was set to 1.0 mils, which fell on the low side of the calculated range. The outer diametric clearances were set to 3.0 mils, just short of the theoretical range. Concurrent researchers were running bearing tests with diametric clearance as low as 0.6 mils for both inner and outer, so the first run values were kept low. These clearances were input into DyRoBeS and the resulting first and second modes were determined. A comparison of experimental and first analytical calculations is shown in Table 4.2.1.

Clearance Calculations for Floating Ring Bearing on the Compressor Side

Coefficients of Thermal Expansion

Steel = $6.5E^{-6}$ in / in * F
Bronze = $10E^{-6}$ in / in * F
Gray Cast Iron = $6.0E^{-6}$ in / in * F

Compressor temperatures: Ambient Temperature - 70F
Shaft - 250 F
Oil - 200 F
Compressor -300 F

Shaft Expansion = D * C_{te} * Δ T
= 0.42" * $6.5E^{-6}$ * (250F-70F)
= 0.49 mils of expansion

Bushing Expansion
=0.5" * $10E^{-6}$ * (200F-70F)
= 0.65 mils expansion

Length Expansion = 1" * 6E-6 * (300F-70F)
= 1.3 mils of expansion

Min Inner Clearance = Min Cold Clearance – Shaft Expansion + Bushing Expansion
= 0.75 - 0.49 + 0.65 = 0.91 mil
Max Max Cold Clearance – Shaft Expansion + Bushing Expansion
= 1.58 - 0.49 + 0.65 = 1.74 mil

Min Outer Clearance = Cold Clearance – Bushing Expansion + Length Expansion
= 2.5 - 0.65 + 1.3 = 3.15 mils
Max Outer Clearance = Cold Clearance – Bushing Expansion + Length Expansion
= 3.4 - 0.65 + 1.3 = 4.05 mils

First run inner clearance for the compressor bearing will be 1.0mils
First run outer clearance for the compressor bearing will be 3.0mils

Figure 4.2.1: Sample calculations for first approximation bearing clearances

Table 4.2.1. First run experimental vs. analytical damped natural frequencies

	Experimental			Analytical		
Bearing Type	1st mode RPM	2nd mode	Run Speed RPM	1st mode RPM	2nd mode RPM	Run Speed RPM
FR	20,000	35,000	97,200	2,300	4,100	100k
6AG	15,000	26,000	96,000	8,000	20,000	100k
8AG	12,000	---	89,250	6,200	13,700	100k
10AG	10,000	---	84,000	5,000	11,490	100k

First run analysis indicated the FR bearing model clearances required adjustment. The FR bearing was the only bearing that had two clearances and, therefore, was the most susceptible to large frequency changes as a result of modeling geometry. As the clearances specified by the blueprints were cold clearances, it was believed that decreasing the clearances would yield more favorable results. Runs were performed with the inner clearances of the FR reduced from 1.0mils to 0.5 mils, 0.4 mils, 0.35 mils, 0.33 mils. These were interchanged on both the compressor and turbine bearings. Results closer matching the experimental data were obtained with both inner and outer bearing clearances set at 0.35 mils. Outer clearance changes below 0.35 mils yielded damped natural frequencies changes that were extreme. The outer clearance remained at 0.35 mils and the inner clearances were varied between 0.33, 0.35, and 0.375, not always equal between the turbine and compressor end. The turbine end experiences higher temperatures, causing thermal expansion, so some test runs were made with the turbine bearing clearances tighter. The raw data for these test runs are located in Appendix B.

Analysis confirmed the expectations that the higher temperatures on the turbine end caused tighter clearances. Final outer clearances were 0.35 mils for both turbine and compressor ends. The inner clearance was set at 0.35 mils for the compressor end, and 0.33 mils for the turbine end. The final results were compared to the experimental in Table 4.2.2. The process was repeated for the 6AG, 8AG, and 10AG bearings, with only the single clearance varied.

Table 4.2.2. Damped natural frequencies for finalized bearing clearances

Bearing Type	Experimental 1st mode RPM	2nd mode RPM	Run Speed RPM	Analytical 1st mode RPM	2nd mode RPM	Run Speed RPM
FR	20,000	35,000	97,200	22,000	38,000	100k
6AG	15,000	26,000	96,000	14,800	31,100	100k
8AG	12,000	---	89,250	13,000	30,000	100k
10AG	10,000	---	84,000	9,000	29,000	100k

After altering the clearances to calibrate the damped natural frequencies at near operating speeds, the first mode damped natural frequency values were read off the waterfall plots at 25k, 50k, and 75k to ensure the calibration was accurate throughout the operating speed range. The resulting data are shown in Table 4.2.3. The table shows strong correlation between the experimental and analytical results throughout the operating speed range and gives confidence that the determined clearance values accurately represent experimental conditions.

Table 4.2.3. Comparison of Damped Natural Frequencies

Mode 1

	25k	50k	75k	100k
FR Experimental	10000	15300	19000	20000
FR Analytical	8700	15000	19000	22000
6AG Experimental	7300	10000	13200	15000
6AG Analytical	6800	9900	12500	14800
8AG Experimental	6100	8400	10000	12000
8AG Analytical	5500	8200	10600	12900
10AG Experimental	6000	7200	8800	10000
10AG Analytical	4200	5800	7200	9000

Back calculations were performed to determine temperatures needed to thermally explain the clearance reduction. A shaft temperature of 350 Fahrenheit results in an inner clearance of 0.35 mils. This temperature is within expectations because the shaft itself is not cooled by the oil bath in the same manner as the bronze bushing. The outer clearance can not be explained by thermal expansion. It is not possible for the 1.25 mil minimum cold clearance to be reduced to 0.35 mils purely on thermal expansion; however it is explained by the non linear nature of the system. What was accomplished by closing the clearances on the bearing was determine stiffness and damping values that provided equivalent damped natural frequencies as the experimental rig. In a linear analysis, the bearing is sitting at a given eccentricity is just spinning. However, in reality, there is a non linear whirling that is known to occur. The non-uniform orbit path caused by the non linear whirling creates stiffness that is larger than would be possible by a shaft that is purely spinning.

Reduction in clearances, for the 6AG, 8AG, and 10AG bearings, increased damped natural frequencies for the first and second modes. This was expected since the lack of space compressed the supporting fluid increased the stiffness and stability. The FR bearing results did not show such a trend. Reducing the outer ring clearance did not noticeably affect the first mode damped natural frequencies, and the second mode frequencies changed randomly. Decreasing the inner ring clearance increased the majority of the first and second mode frequencies, as expected, however there were multiple data points that did not follow this trend. Clearance adjustments were primarily for calibration to the experimental results. A thorough study of various inner and outer clearances for both bearings would be beneficial at a future date.

4.3 Influence of Compressor Loading on Bearing Eccentricity

Bearing eccentricity refers to the movement experienced by the bearing towards the housing wall. An eccentricity of 1.0 would represent the bearing hitting the wall, causing damage to the bearing and housing. Acceptable eccentricities were considered anything below 95 percent (0.95). Data collected from the BePerf software showed that 15 pounds of compressor loading caused the 8AG bearing to reach maximum safe performance limit. Above 15lbs the eccentricity would be greater than the allowable 0.95 eccentricity. The 6AG and FR bearings, both compressor and turbine ends, could handle up to 25 pounds loading without risk of damage. Additional runs were attempted, but the software was unable to converge to a solution beyond 25 pounds of load for the 6AG bearing. The loading values and the resulting eccentricities are shown in Table 4.3.1

Table 4.3.1. Summary Table for Loading affects on Bearing Eccentricity

FR Turbine End		FR Compressor End		6AG Compressor End		8AG Compressor End	
Load	Eccentricity	Load	Eccentricity	Load	Eccentricity	Load	Eccentricity
0	0.041	0	0.002	0	0.035	0	0.065
5	0.128	5	0.117	5	0.553	5	0.622
10	0.208	10	0.211	10	0.687	10	0.811
15	0.27	15	0.268	15	0.725	15	0.892
20	0.328	20	0.327	20	0.781		
25	0.37	25	0.404	25	0.796		

In figure 4.3.1 clear trend lines show the rate of change of eccentricity as a function of the load placed on the compressor wheel. The floating ring bearings had linear rate of increase due to compressor loading. The 6AG and 8AG bearings experienced more drastic change as loading began, but leveled out beyond approximately

eight pounds. The solution for the 10AG was unable to converge above 1.5lbs loading, so the resulting trend line is shorter but clearly showed the 10AG approaching an unacceptable eccentricity.

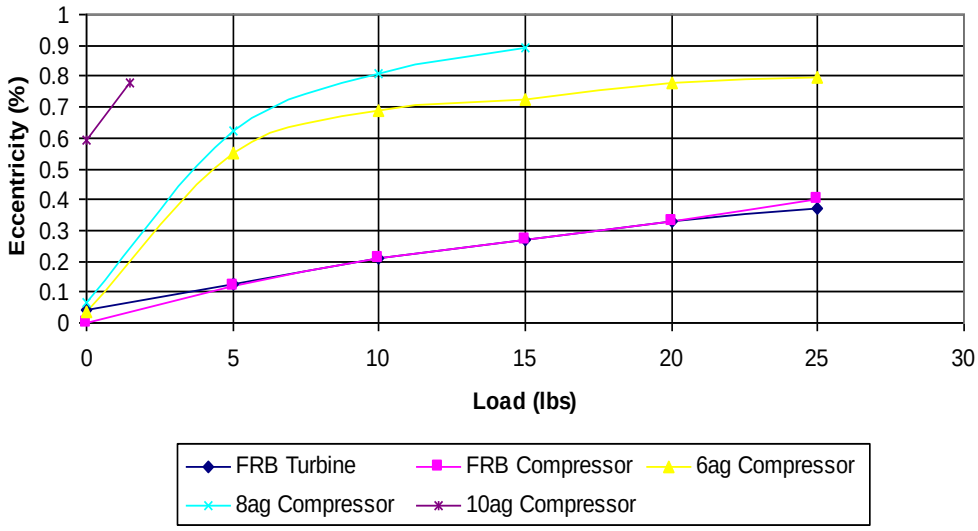

Figure 4.3.1 Trend lines for eccentricity as a function of loading

4.4 Influence of Turbocharger Speed on Stability

For all bearing types, the damped natural frequencies increased with turbocharger shaft speed. First and second mode frequencies showed significant increase as the turbocharger shaft speed increases. No first or second mode frequencies crossed from unstable to stable as the result of an increase in shaft speed. Table 4.4.1 and Figure 4.4.1 show the influence of turbocharger shaft speed on the damped natural frequencies for the FR bearing. While first performed on the unloaded cases, similar trends were later observed through all loading conditions. Tables and Figures for the 6AG, 8AG, and 10AG bearings are located in Appendix C.

Table 4.4.1. Influence of shaft speed on unstable damped natural frequencies

	FR Mode1	FR Mode 2	6AG Mode 1	6AG Mode 2	8AG Mode 1	8AG Mode 2	10AG Mode 1	10AG Mode 2
25000	8691		6719		5503		4256	
50000	14546		9884	18033	8225	17682	5807	17348
75000	18875	28830	12478	25436	10642	24705	7199	24087
100000	22371	37966	14876	31130	12906	30067	8478	29170
125000	25419	45969	17420	35777	15081	34430	9676	33264
150000	28171	52391	19627	39600	17200	38195	10813	36759

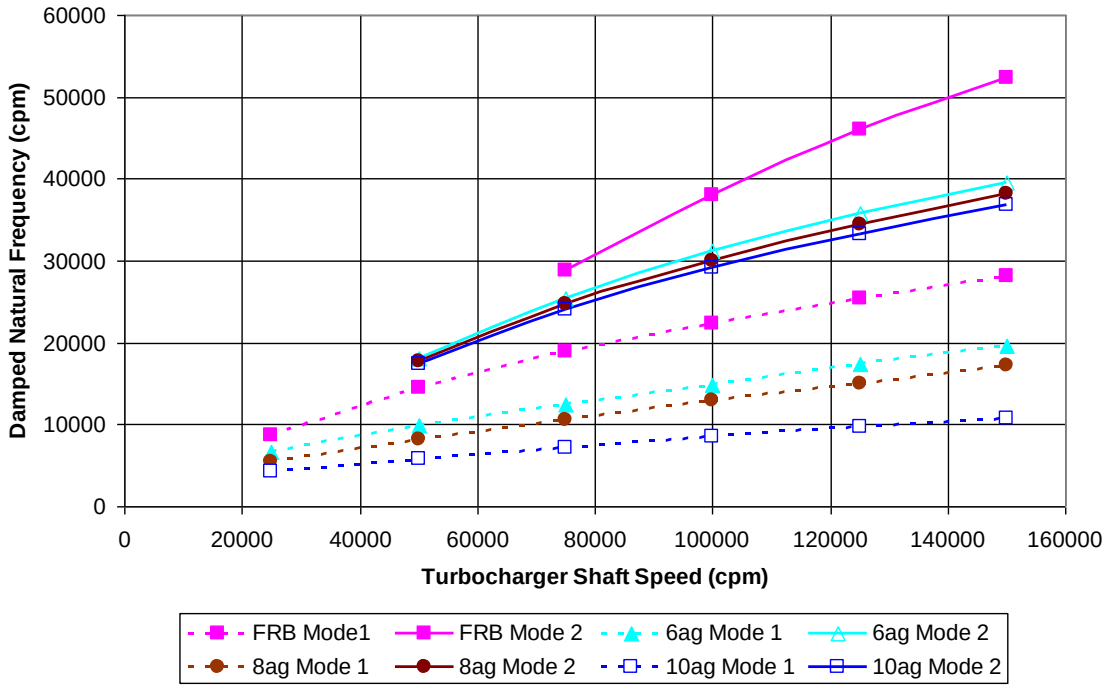

Figure 4.4.1: Influence of shaft speed on damped natural frequencies.

The log decrement values output by DyRoBeS provide a numerical representation of the stability of the bearing. Negative log decrement values represent unstable modes while positive represent stable. In a linear sense, a negative log decrement means that the instability continues to grow infinitely, representing total failure of the rotor bearing system. This is explained by the linear analysis being used. In real operation, there is a non linear limit cycle that prevents the instability from growing infinitely.

The first and second unstable modes were plotted for the FR and 6AG bearings and are displayed in Figures 4.4.2 and 4.4.3 respectively. Both first and second mode trends for the FR show that as the turbocharger shaft speed increases, the log decrement decreases meaning the rotor bearing system becomes more unstable. The same trend was observed for the second mode of the 6AG, however the first mode became increasingly less stable at speeds above 100k RPM. The 8AG and 10AG bearings showed similar trends to the FR in both first and second modes. Stability maps were generated to show both stable and unstable modes for the unloaded FR, 6AG, 8AG, and 10AG bearings and are found in Appendix D.

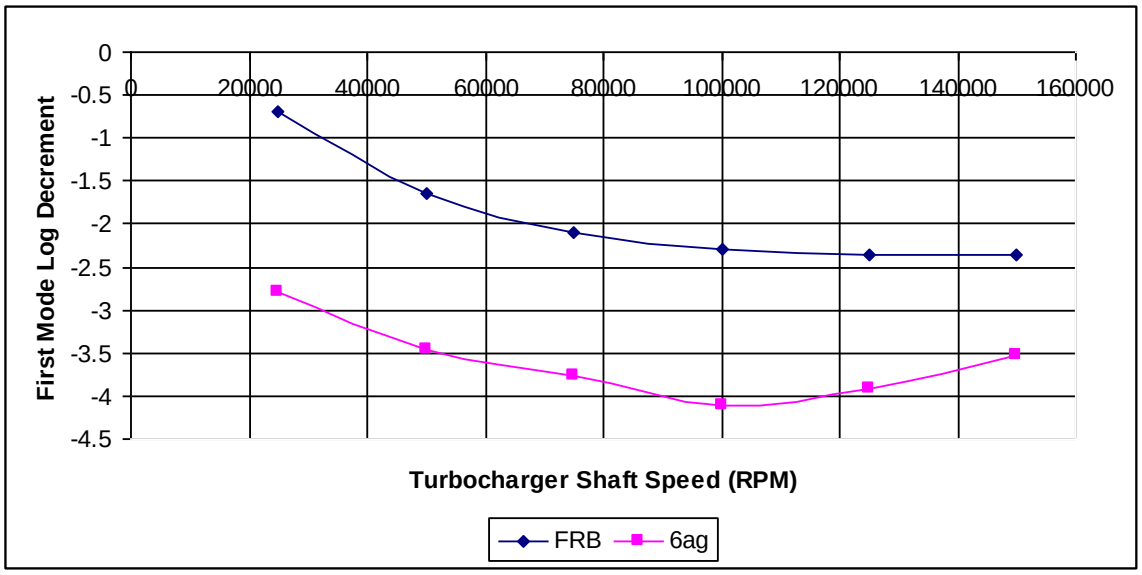

Figure 4.4.2: Influence of shaft speed on first mode stability

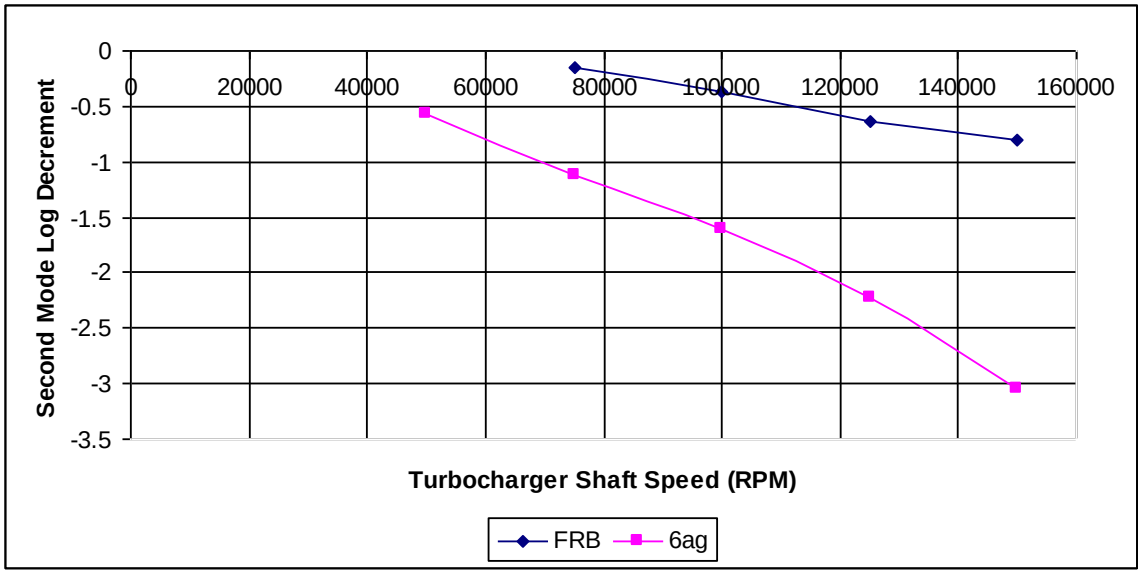

Figure 4.4.3: Influence of shaft speed on second mode stability

Turbocharger shaft speed influences the mode shapes of all four experimental bearings. For the FR, the first mode shapes showed a rigid conical trend. This changed only slightly as speed is increased, moving toward small bending of the shaft on the turbine end. The second mode changed substantially. The original cylindrical mode moved into heavy bending with the turbine bearing becoming pinned. The first and second modes for the FR are shown in Figures 4.4.3 and in Figures 4.4.4 respectively.

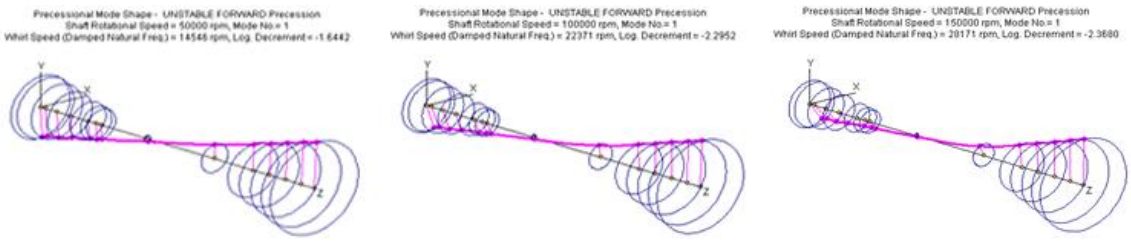

Figure 4.4.4: FR 1st mode shapes based on increasing speed (50k, 100k, 150k)

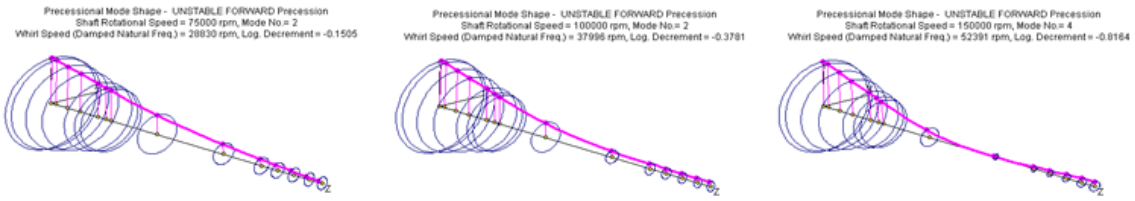

Figure 4.4.5: FR 2nd mode shapes based on increasing speed (50k, 100k, 150k)

The 8AG and 10AG results were nearly identical, showing slight change in the first mode, and similar development of bending in the turbocharger shaft at high speed. The 6AG case did not show the same trend as the others, and exhibited strong response to increased turbocharger shaft speed. The low speed runs of 50k and 100k RPM were consistent with the other bearing cases. The first and second mode showed a marked change at 150k RPM. The overall mode shape moved away from the conical first mode and into a bending mode on the compressor and turbine end of the shafts. The second mode shape changed significantly at 150k RPM, with both bearings becoming pinned. Importantly, the 6AG second mode suddenly developed a large amount of bending compressor side of the shaft. This trend was not seen for any other cases. Bearing files and rotor models were double checked to determine whether these anomalies were the result of input error. These runs provided identical results. The mode shapes for the 6AG and 8AG are shown in Figures 4.4.4 through 4.4.7, and the figures for the 10AG are found in Appendix D.

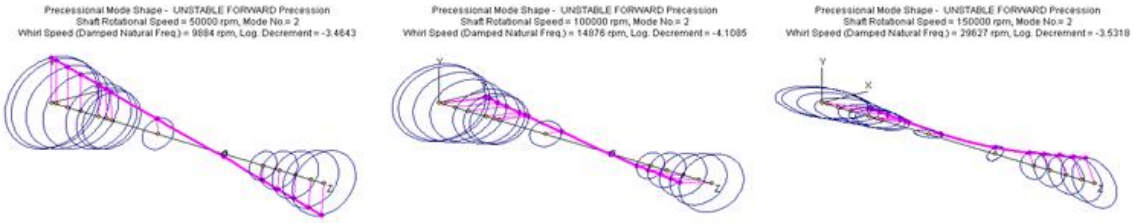

Figure 4.4.6: 6AG 1st mode shapes based on increasing speed. (50k, 100k, 150k)

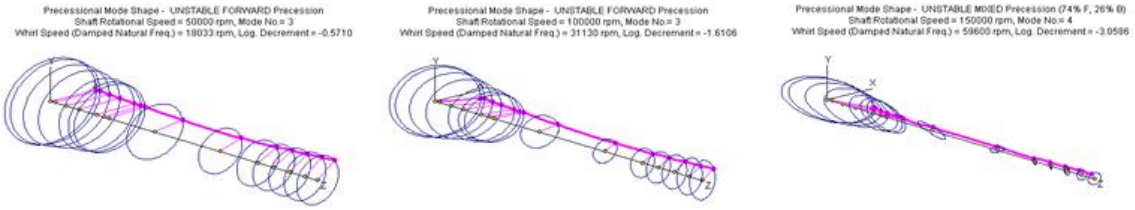

Figure 4.4.7: 6AG 2nd mode shapes based on increasing speed (50k, 100k, 150k)

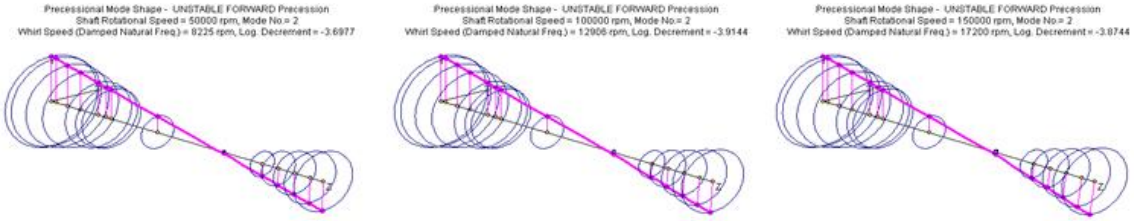

Figure 4.4.9: 8AG 1st mode shapes based on increasing speed (50k, 100k, 150k)

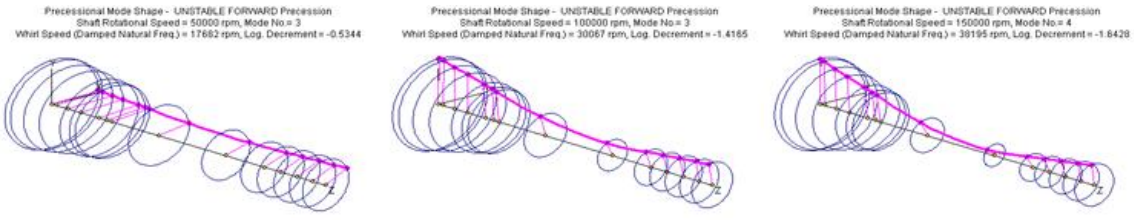

Figure 4.4.9: 8AG 2nd mode shapes based on increasing speed (50k, 100k, 150k)

4.5 Influence of Axial Grooves on Stability

Analysis of the influence of axial grooves number on the damped natural frequencies of the turbocharger showed that increasing the number of axial grooves is detrimental to turbocharger stability. The gravity load plots of first and second mode frequencies as a function of axial groove number are shown below in Figures 4.5.1 and 4.5.2.

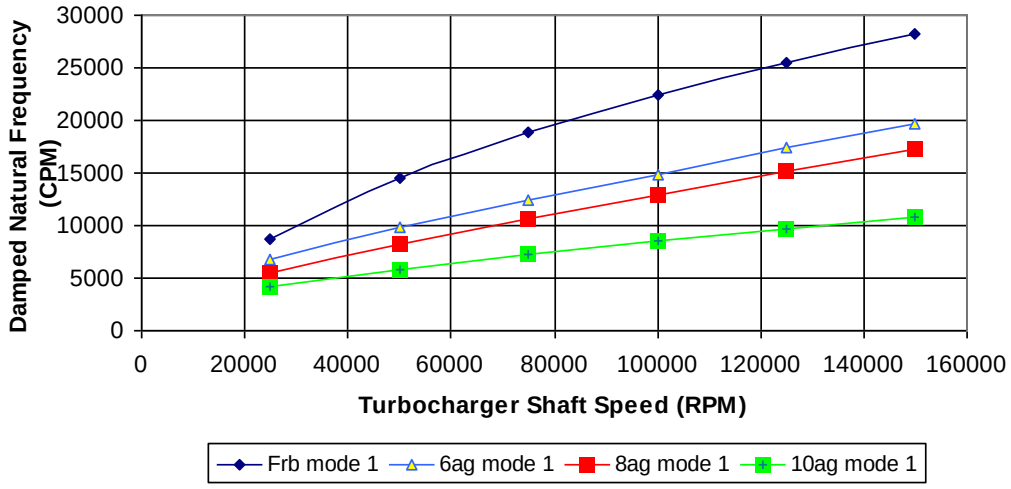

Figure 4.5.1 Influence of axial grooves on 1st mode damped natural frequencies

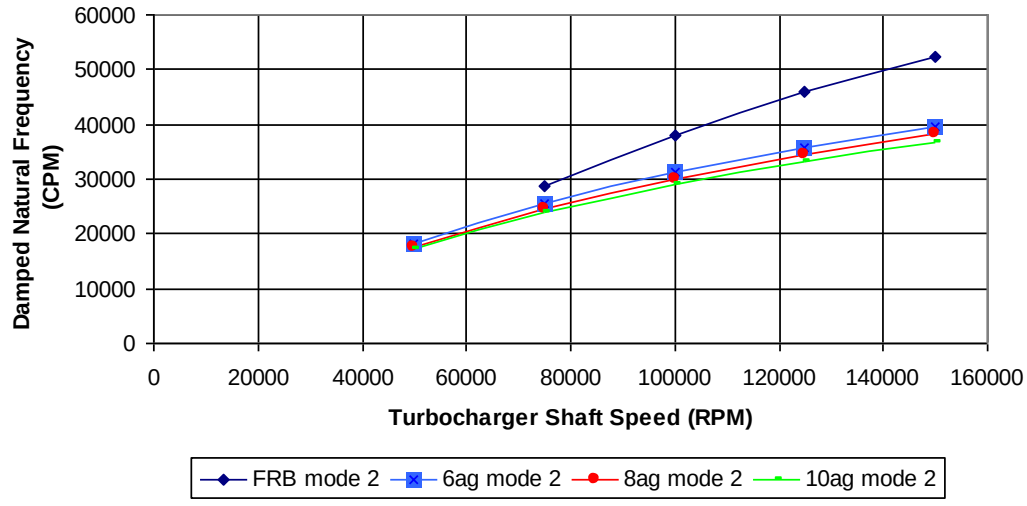

Figure 4.5.2: Influence of axial grooves on second mode damped natural frequencies.

The plots demonstrate the FR (0 axial grooves) had the highest damped natural frequencies, followed in order by the 6AG, 8AG, and 10AG bearings. In addition, the first mode frequencies were more affected by the number of axial grooves than were the second mode. While there was only a slight change in the second mode frequencies between the 6AG, 8AG, and 10AG bearings, the FR had noticeably higher damped natural frequencies. A similar trend was noted in all of the loaded cases. Data for 5, 10, 15, 20, and 25 pound loads are found in Appendix D.

Each bearing type's log decrements were over plotted for both first and second modes. The floating ring bearing was significantly closer to stable for the first and second modes than any of the grooved bearings. For the first mode, the number of the axial grooves has a negligible affect on the stability of the rotor shaft system. The second mode showed a similar pattern. The FR was far superior in minimizing instability. The 8 and 10AG bearings performed similarly however the 6AG had a marked increase in instability beginning 100,000 RPM. The log decrement values are shown in Table 4.5.1 and the first and second mode unstable log decrement values are displayed in Figure 4.5.3 and Figure 4.5.4 respectively. Table 4.5.1 indicates that the FR bearing is more stable than any of the axial groove bearings for both first and seconds modes throughout the operating speed range.

Table 4.5.1. Log decrement values for unloaded condition.

Speed	FRB		6ag		8ag		10ag	
RPM	1st mode log dec	2nd mode log dec	1st mode log dec	2nd mode log dec	1st mode log dec	2nd mode log dec	1st mode log dec	2nd mode log dec
25k	-0.6916		-2.8		-3.1		-2.97	
50k	-1.6442		-3.46	-0.57	-3.69	-0.53	-3.6	-0.51
75k	-2.09	-0.15	-3.76	-1.12	-3.86	-1.07	-3.78	-1.05
100k	-2.29	-0.37	-4.1	-1.61	-3.91	-1.41	-3.82	-1.38
125k	-2.36	-0.63	-3.92	-2.22	-3.91	-1.58	-3.81	-1.54
150k	-2.36	-0.81	-3.53	-3.05	-3.87	-1.64	-3.77	-1.58

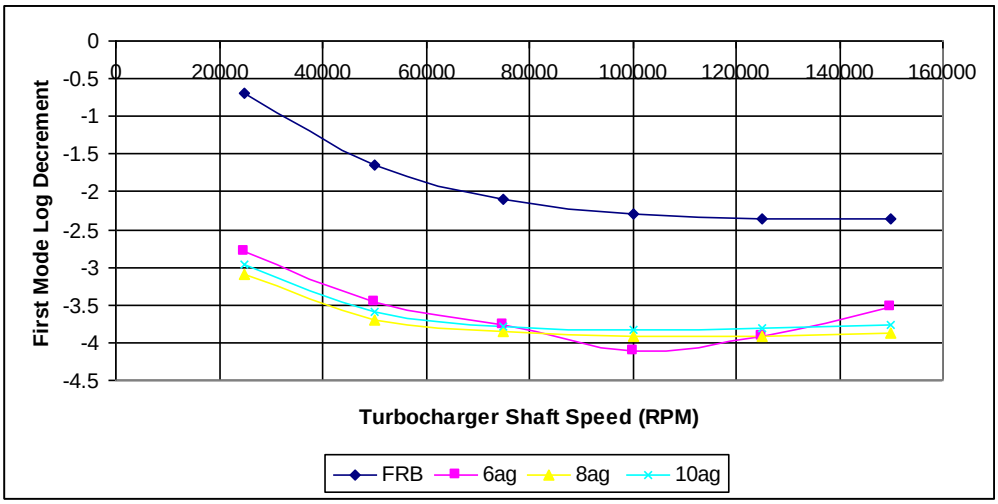

Figure 4.5.3: Influence of axial grooves on first mode log decrement

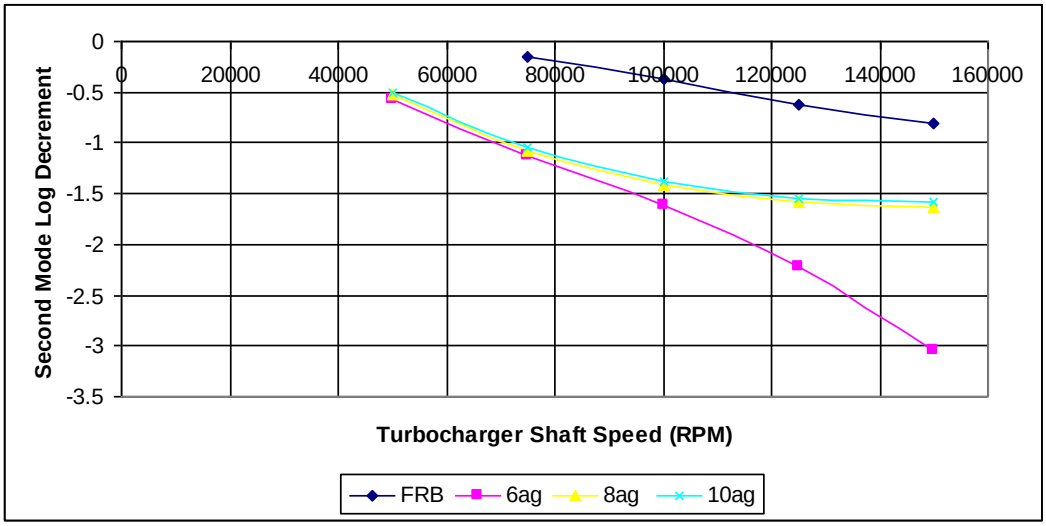

Figure 4.5.4: Influence of axial grooves on second mode log decrement

4.6 Influence of Compressor Loading on Stability

All bearing types showed that as the compressor loading increased, the damped natural frequencies increased. In addition to an increase in the damped natural frequencies, many of the first and second mode frequencies that were unstable for the unloaded condition stabilized as the loading was increased. In the charts below, red values represent a frequency that was previously unstable at gravity load.

At low loads for the FR bearing, the damped natural frequency increase was approximately six percent for each five pound increase in compressor loading. However, as the loading increased, the amount of benefit for further loading began to decrease . Table 4.6.1 displays the results of the loaded test runs. Similar trends were noted for the 6AG and 8AG cases, the data and figures are found in Appendix E.

Table 4.6.1. 1st and 2nd mode frequencies for the FR bearing under compressor load.
Red value in **bold** *italic* was a frequency that was previously unstable at gravity load.

FR	Mode 1					
	Unloaded	5lb	10lb	15lb	20lb	25lb
25000	8691	9908	***11056***	***12020***	***12923***	***13483***
50000	14546	15199	16588	17877	18822	19574
75000	18875	18815	19895	21203	22467	23231
100000	22371	22808	23196	24020	24999	25935
125000	25419	24750	25690	26662	27324	28059
150000	28171	27462	27947	28999	29701	30188
	Mode 2					
	Unloaded	5lb	10lb	15lb	20lb	25lb
25000						
50000						
75000	28830	26930	***28705***	***30365***	***31906***	***32970***
100000	37966	34432	36479	***38118***	***39765***	***39856***
125000	45969	40744	42396	44263	45583	47273
150000	52391	46232	47055	48869	49999	51316

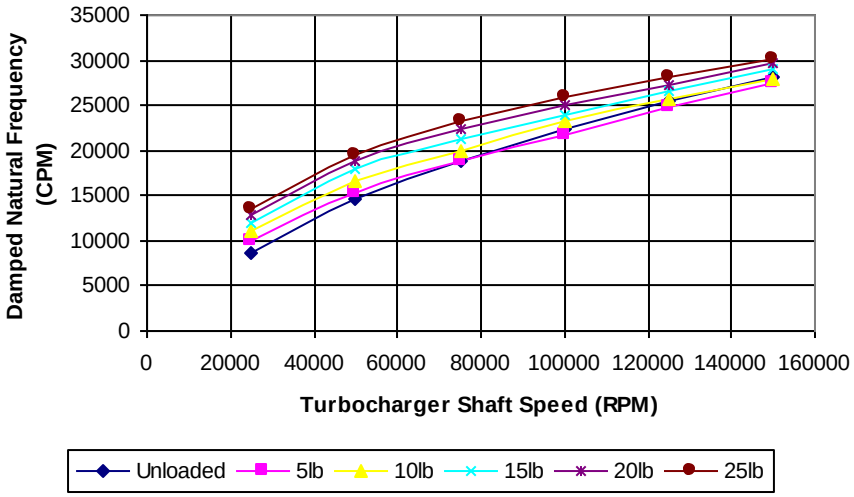

Figure 4.6.1: 1st mode damped natural frequencies for loading of FR bearing

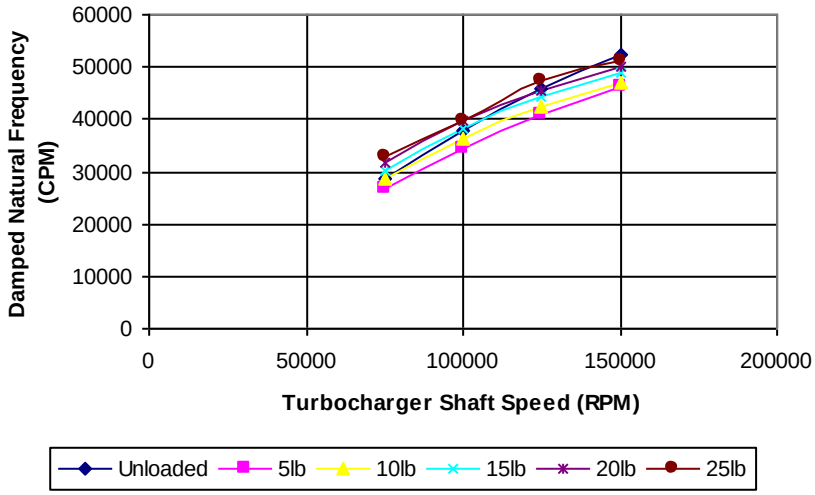

Figure 4.6.2: Second mode damped natural frequencies for loading of FR bearing

Loading of the compressor wheel significantly impacted the stability of each of the bearing types. As loading was applied to the FR bearing, the 2nd mode instability began to disappear. The remaining unstable log decrements were reduced to near zero representing a move towards stable. The 6AG bearing saw similar benefit from the

addition of compressor loading. Many of the second mode instabilities disappeared, especially at lower shaft speeds, while the remaining unstable log decrements became closer to stable. Under higher loading and higher speeds the first and second mode log decrement values were near identical, however, under lower speed and loads (representative of start up conditions in real world operation), the FR bearing proved to be more stable than the 6AG. Figure 4.6.2 through Figure 4.6.3 show the influence of loading on the first and second modes of the FR and 6AG. The stability maps showing both stable and unstable log decrements for the loaded cases are found in Appendix E.

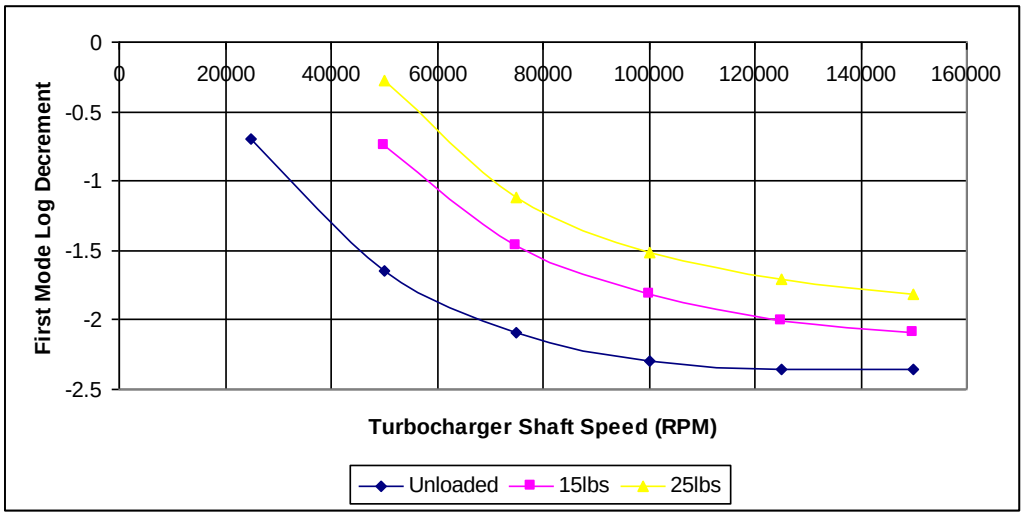

Figure 4.6.3. Influence of loading on first mode stability of floating ring bearing

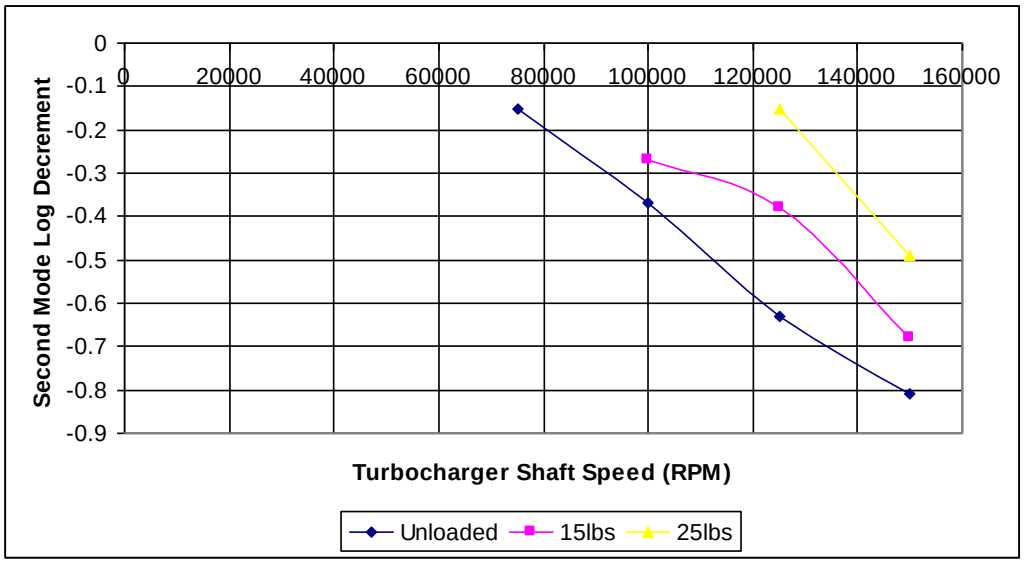

Figure 4.6.4. Influence of loading on second mode stability of floating ring bearing

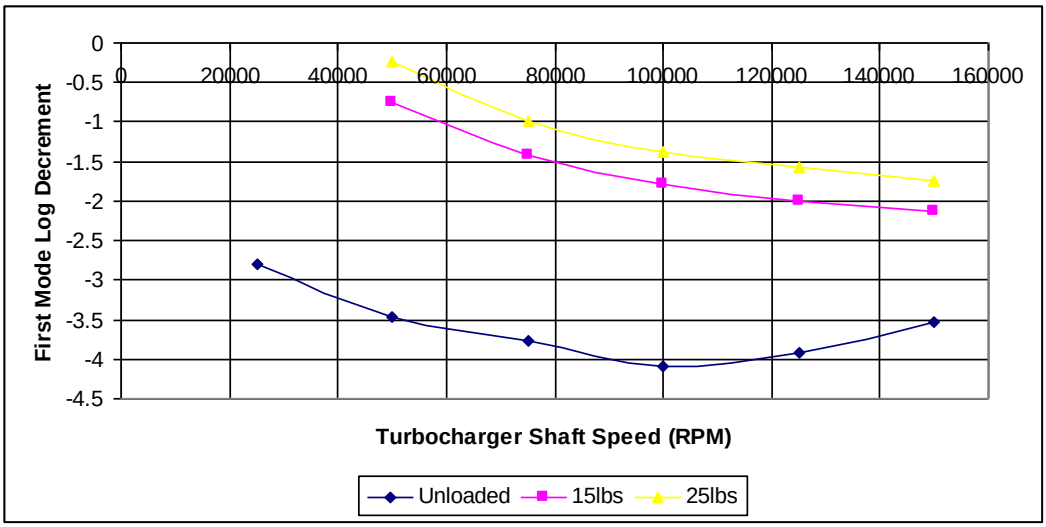

Figure 4.6.5. Influence of loading on first mode stability of 6AG bearing

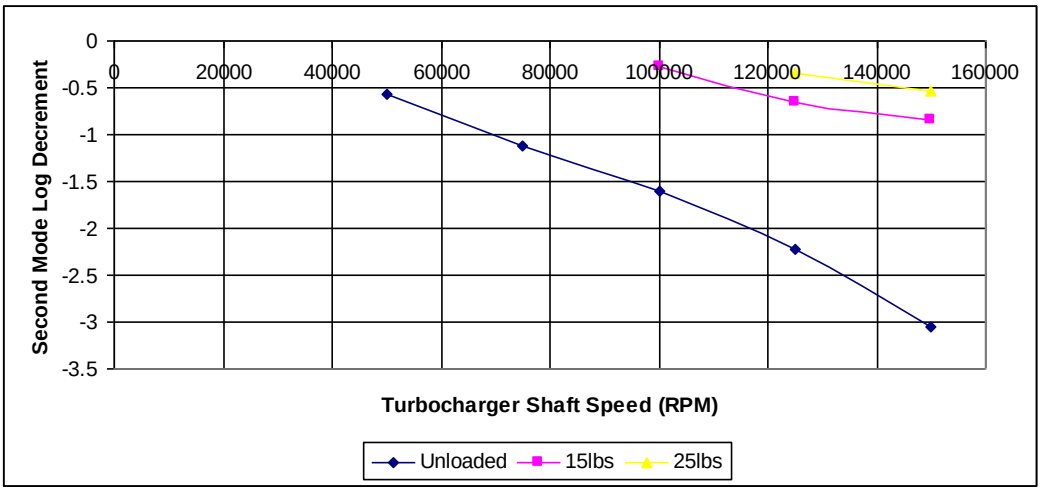

Figure 4.6.6. Influence of loading on second mode stability of 6AG bearing

The first mode shapes of the floating ring bearing remained constant through the load range. The second mode showed that the increasing the load on the compressor wheel caused the shaft to bend and ultimately pin on the turbine end at 25lbs of compressor load. Though stable at these loads, the trend should be monitored closely to prevent damage to the turbocharger shaft. The mode trends are shown for the various compressor loads, at 100k CPM, in Figures 4.6.3 and Figure 4.6.4.

The 6AG and 8AG showed similar changes in mode shape based on loading. First mode shapes remained consistent with increased loading, while the second mode moved towards being pinned on the turbine side. Mode shape progressions for 6AG and 8AG bearings are found in Appendix E.

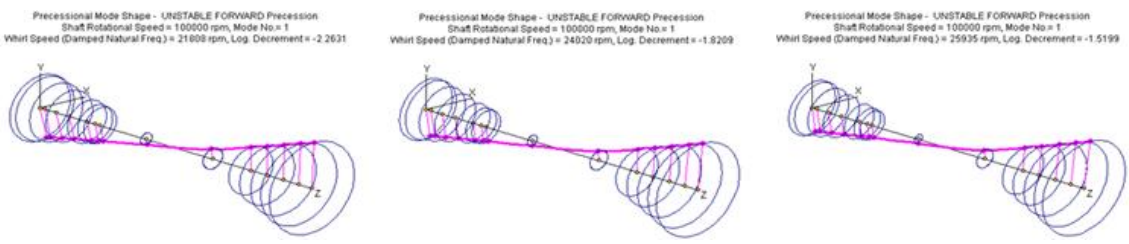

Figure 4.6.7: FR bearing 1st mode shape with increased loading (5lb, 15lb, 25lb)

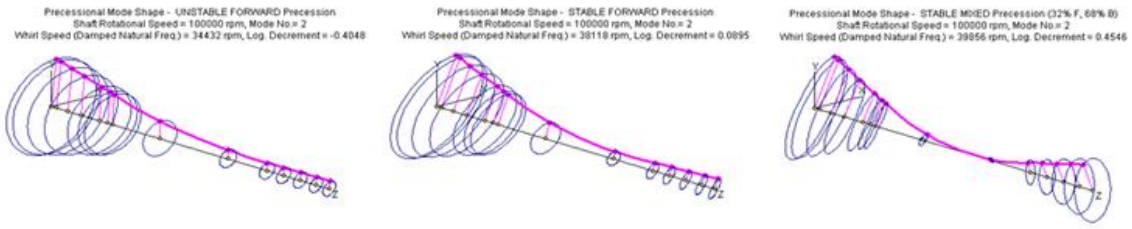

Figure 4.6.8: FR bearing 2nd mode shape with increased loading (5lb, 15lb, 25lb)

4.7 Conclusions

Automotive turbochargers experience self-excited instability through their operating range. Reducing these instabilities is a primary concern in industry due to the high cost of replacing turbocharger components, in terms of both time and cost. Custom designed axial groove bearings were tested analytically with the goal of understanding and reducing self-excited instability while maintaining or increasing performance.

Analytical unloaded runs provided similar insight to the experimental frequency content of the FR, 6AG, 8AG, and 10AG bearings. The current DyRoBeS turbo and bearing files will provide accurate predictions for high speed and high load, stability analysis.

Many factors influenced the damped natural frequencies and stability of the bearings. The largest influence resulted from modifying the bearing clearance geometry. Since the precise clearances are unknown, iterative processes were used to calibrate the analytical model to experimental results for unloaded test runs. Varying the clearances with even slight changes, tenths of mils, made significant impacts on first and second mode instabilities.

The axial groove number in the bearing also played a large role in high speed instability. Preliminary testing suggested 8AG and 10AG bearings were both too unstable, even under minimal load conditions. This research showed the addition of grooves resulted in a decrease in the stability through the operating speed range. The 6AG bearing performed the best of the axial groove bearings. However, the damped natural frequencies, while unloaded, still remained well below those of the FR bearing.

Increasing the engine speed increased the damped natural frequencies of all of the bearing types; however the overall stability decreased with engine speed. As the engine speed increased incrementally to 150k RPM, the damped natural frequencies increased as well. None of the first or second mode instabilities disappeared with increased speed. Increased compressor loading, representative of the actual work done by the turbocharger during field operation, played a more significant role in reducing instabilities. With 25lbs of compressor loading, the FR bearing eliminated first mode instability at low speed, below 50k RPM, and two second mode instabilities below 100k RPM. The 6AG bearing also benefited but the second mode instabilities were eliminated only up to 75k RPM. Compressor loading increased the stability of all bearing types. The 6AG and 8AG bearings performed similarly with 15lbs of compressor loading, however the 8AG was unable to be loaded to 25lbs, and the 6AG was unable to match the performance of the floating ring bearing.

Despite the improved performance of the 6AG bearing with compressor loading, linear analytical testing shows it fails to outperform the stock FR bearing currently used in production turbochargers.

Chapter 5

Future Work

5.1 Recommendations for Future Work

The results of this research showed that the largest influence on the analytically determined first and second mode instabilities was the bearing clearances used in the models. Small clearance changes, a tenth of a mil, resulted in a marked increase in the damped natural frequencies.

The FR bearing had two clearances on both the compressor and turbine sides of the rotor shaft. While preliminary testing showed decreasing the inner and outer clearances increased stability, many data points fell outside this trend. A thorough study should be performed to detail the influence of bearing geometry. It is recommended that the inner and outer clearances be tested at 0.75, 0.50, 0.40, 0.35, and 0.33 mils on the compressor end, and 0.70, 0.45, 0.35, 0.33, and 0.31 mils on the turbine end. The smaller clearances on the turbine end result from higher temperatures experienced causing greater expansion of the bearing material. A full study would enable the analytical model to better match the experimental data, and improve calibration for high speed instability predictions.

Shaft temperatures should be investigated as an extension to this research in order to calculate thermal expansion. No method exists for determining the internal temperatures of the lubricant film and turbocharger shaft within the housings. Current estimates use a thermal sensor on the turbine and compressor wheel housings, but do not account for heat dissipation through the oil film. Determining shaft temperatures is

complicated by the inability to install instrumentation inside of the housings without interfering with the operation of the turbocharger.

Other types of bearings could yield an acceptable alternative to the stock floating ring bushings FR bearing found in most automotive turbochargers. Recently, air bearings and ball bearing have begun to see use and could be viable options to reduce self-excited instabilities. While DyRoBeS software does not have the capability to analyze these bearing types other FEA based programs, such as ADINA (Automatic Dynamic Incremental Nonlinear Analysis), have this ability.

Should an acceptable bearing type be found to replace the FR bearing based on stability findings, additional studies must be performed to ensure the bearing can perform under real world circumstances. An endurance study will be required to ensure the bearing can perform reliably over a large number of start-up, operation, and spin down cycles. Also, shock loads, such as hitting a pot hole while driving, must be modeled and tested to ensure the turbo will not fail due to acute vibration sources.

References

[1] Watson, N. and Janota, M. S., 1982, Turbocharging the Internal Combustion Engine, Wiley, New York.

[2] Gunter, Kirk, Alsaed (2007), "Stability Analysis of A High Speed Automotive Turbocharger," Mortimer House, London, UK

[3] Kirk, R. G., Alsaeed, A., Liptrap, J., Lindsey, C., Sutherland, D., Dillon, B., Saunders, E., Chappell, M., Nawshin, S., Christian, E., Ellis, A., Mondschein, B., Oliver, J., and Sterling, J., "Experimental Test Results for Vibration of a High Speed Diesel Engine Turbocharger," Tribology Transactions, 51(4), 2008, pp 422 - 427.

[4] Kirk, Kornhauser, Sterling, Alsaeed (2007) "High Speed Turbocharger Instability", *Proc ISCORMA 4*, Alberta, Canada

[5] Holmes, R., Brennan, M. J. and Gottrand, B., 2004, "Vibration of an Automotive Turbocharger – A Case Study," Proc. 8th International Conference on Vibrations in Rotating Machinery, Swansea, UK, pp. 445-450.

[6] Alsaeed, (2005), "Dynamic Stability Evaluation of an Automotive Turbocharger Rotor-Bearing System", M.S. Thesis, Virginia Tech Libraries, Blacksburg, VA

[7] Tanaka, M., Hatakenaka, K. and Suzuki, K., "A Theoretical Analysis of Floating Bush Journal Bearing with Axial Oil Film Rupture Being Considered", Trans. ASME Journal of Tribology, Vol. 124, 2002, pp. 494-505.

[8] Kirk, Sterling et al (2007), "Diesel Engine Turbocharger Rebuild and Experimental Testing", *Proc. of the STLE/ASME International Joint Tribology Conference*, San Diego, CA.

[9] Sterling, (2009), “Influence of Induced Unbalance on Subsynchronous Vibrations of an Automotive Turbocharger”, M.S. Thesis, Virginia Tech Libraries, Blacksburg, VA

[10] Harnoy, Avraham. 2003, “Bearing Design in Machinery”, Marcel Dekker Inc, New York.

[11] Pettinato, (2003) “Rotordynamic and Bearing Upgrade of a High-Speed Turbocharger”, *Journal of Engineering for Gas Turbines and Power*, Jeanette, PA.

[12] Agrawal (1997), “Foil Air/Gas Bearing Technology – An Overview”, *American Society of Mechanical Engineers*, New York City, NY.

[13] Gunter, E. G. and Chen, W. J., 2000, DyRoBeS© - Dynamics of Rotor Bearing Systems User’s Manual, RODYN Vibration Analysis, Inc., Charlottesville, VA.

[14] Gunter, E.G. and Chen, W.J.(2005),“Dynamic Analysis of a Turbocharger in Floating Bushing Bearings,” *Proc.3rd International Symposium on Stability Control of Rotating Machinery*, Cleveland, OH.

[15] Kirk, Mondschein, Alsaeed et al (2010), “Influence of Turbocharger Bearing Design on Observed Linear and Nonlinear Vibration,” *Proc. STLE/ASME 2010 International Joint Tribology Conference*, San Francisco, CA.

Appendix A

Thermodynamic Expansion Calculations for Bearing Clearances

Clearance Calculations for Floating Ring Bearing on the Compressor Side

Coefficients of Thermal Expansion

Steel = $6.5E^{-6}$ in / in * F
Bronze = $10E^{-6}$ in / in * F
Gray Cast Iron = $6.0E^{-6}$ in / in * F

Compressor temperatures: Ambient Temperature - 70F
Shaft - 250 F
Oil - 200 F
Compressor -300 F

Shaft Expansion = D * C_{te}* Δ T
= 0.42" * $6.5E^{-6}$ * (250F-70F)
= 0.49 mils of expansion

Bushing Expansion
=0.5" * $10E^{-6}$ * (200F-70F)
= 0.65 mils expansion

Length Expansion = 1" * 6E-6 * (300F-70F)
= 1.3 mils of expansion

Min Inner Clearance = Min Cold Clearance – Shaft Expansion + Bushing Expansion
= 0.75 - 0.49 + 0.65 = 0.91 mil
Max Max Cold Clearance – Shaft Expansion + Bushing Expansion
= 1.58 - 0.49 + 0.65 = 1.74 mil

Min Outer Clearance = Cold Clearance – Bushing Expansion + Length Expansion
= 2.5 - 0.65 + 1.3 = 3.15 mils
Max Outer Clearance = Cold Clearance – Bushing Expansion + Length Expansion
= 3.4 - 0.65 + 1.3 = 4.05 mils

First run inner clearance for the compressor bearing will be 1.0mils
First run outer clearance for the compressor bearing will be 3.0mils

Clearance Calculations for Floating Ring Bearing on the Turbine Side

Coefficients of Thermal Expansion

Steel = $6.5E^{-6}$ in / in * F
Bronze = $10E^{-6}$ in / in * F
Gray Cast Iron = $6.0E^{-6}$ in / in * F

Turbine temperatures: Ambient Temperature - 70F
- Shaft - 350 F
- Oil - 300 F
- Compressor - 400 F

Shaft Expansion = D * C_{te} * Δ T
= 0.42" * $6.5E^{-6}$ * (350F-70F)
= 0.764 mils of expansion

Bushing Expansion
=0.5" * $10E^{-6}$ * (300F-70F)
= 1.15 mils expansion

Length Expansion = 1" * 6E-6 * (400F-70F)
= 1.8 mils of expansion

Min Inner Clearance = Min Cold Clearance – Shaft Expansion + Bushing Expansion
= 0.75 - 0.764 + 1.15 = 1.13 mil
Max Outer Clearance = Max Cold Clearance – Shaft Expansion + Bushing Expansion
= 1.58 - 0.764 + 1.15 = 1.97 mil

Min Outer Clearance = Cold Clearance – Bushing Expansion + Length Expansion
= 2.5 – 1.15 + 1.8 = 3.15 mils
Max Outer Clearance = Cold Clearance – Bushing Expansion + Length Expansion
= 3.4 - 1.15 + 1.8 = 4.05 mils

First run inner clearance for the turbine bearing will be 1.0 mils
First run outer clearance for the turbine bearing will be 3.0 mils

Appendix B

Bearing Clearance vs. Frequency Data

Table B.1. Raw data for clearance vs. damped natural frequency

RUN 1 Co = .0035 for both

ci = .00035 compressor, .000033 turbine

Comp	Di - .4328	Do - .6253
Turbine	Di - .43276	Do - .6253

Mode 1	22371
Mode 2	37996

RUN 2 Co = .0035 for both

ci = .00035 compressor, .000035 turbine

Comp	Di - .4328	Do - .6253
Turbine	Di - .4328	Do - .6253

Mode 1	22534
Mode 2	38181

RUN 3 Co = .0035 for both

ci = .000375 compressor, .000035 turbine

Comp	Di - .43285	Do - .6253
Turbine	Di -.43276	Do - .6253

Mode 1	22544
Mode 2	39845

RUN 4 Co = .0035 for both

ci = .00035 compressor, .000035 turbine

Comp	Di - .4328	Do - .6253
Turbine	Di -.4328	Do - .6253

Mode 1	22574
Mode 2	40023

Table B.2. Raw data for 6AG and 8AG clearance changes.

	.50-6AG		.50-8AG	100k	75k
	Mode1	20318	Mode1	18340	15332
	Mode2	35389	Mode2	32717	26602
	.75-6AG		**.75-8AG**	**100k**	**75k**
	Mode1	**14876**	**Mode1**	**14876**	**12478**
100k	**Mode2**	**31130**	**Mode2**	**31130**	**25346**
	.90-6AG		.90-8AG	100k	75k
	Mode1	12132	Mode1	10781	8850
100k	Mode2	30419	Mode2	29557	24334

Appendix C

Influence of Compressor Load on Bearing Eccentricity

Table C.1. Bearing eccentricity as a function of load for FR, 6AG, 8AG bearings

FR Turbine End		FR Compressor End		6AG Compressor End		8AG Compressor End	
Load	Eccentricity	Load	Eccentricity	Load	Eccentricity	Load	Eccentricity
0	0.041	0	0.002	0	0.035	0	0.065
5	0.128	5	0.117	5	0.553	5	0.622
10	0.208	10	0.211	10	0.687	10	0.811
15	0.27	15	0.268	15	0.725	15	0.892
20	0.328	20	0.327	20	0.781		
25	0.37	25	0.404	25	0.796		

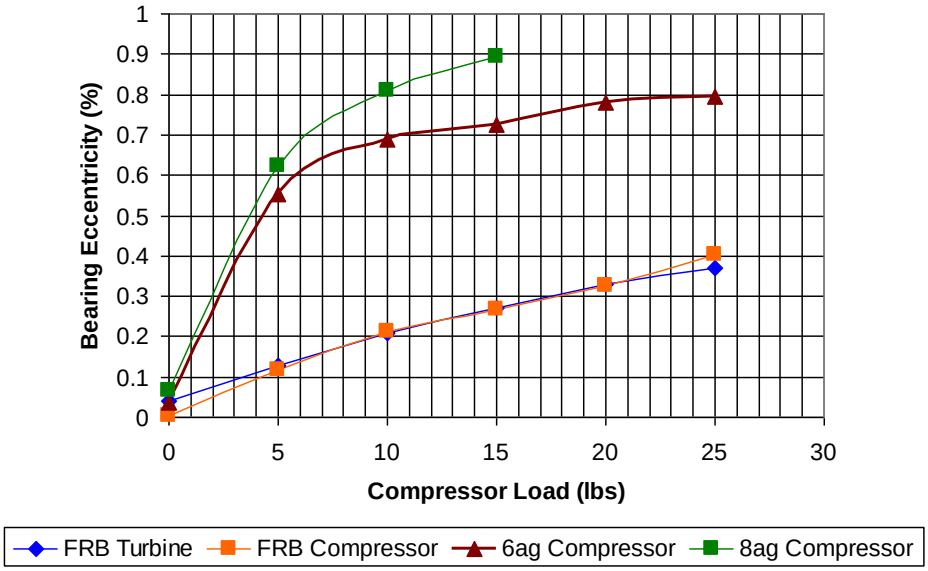

Figure C.1. Compressor end bearing eccentricity versus load

Appendix D

Influence of Turbocharger Shaft Speed on Damped Natural Frequency Data

Table D.1. Influence of shaft speed on damped natural frequencies.

	FR Mode1	FR Mode 2	6AG Mode 1	6AG Mode 2	8AG Mode 1	8AG Mode 2	10AG Mode 1	10AG Mode 2
25000	8691		6719		5503		4256	
50000	14546		9884	18033	8225	17682	5807	17348
75000	18875	28830	12478	25436	10642	24705	7199	24087
100000	22371	37966	14876	31130	12906	30067	8478	29170
125000	25419	45969	17420	35777	15081	34430	9676	33264
150000	28171	52391	19627	39600	17200	38195	10813	36759

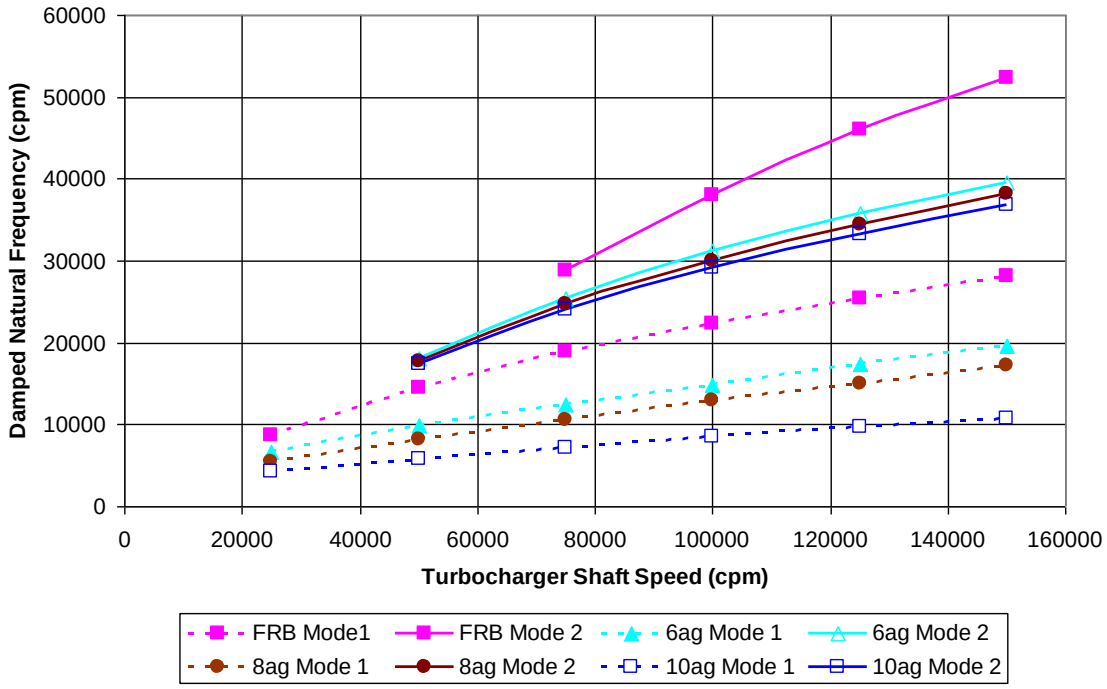

Figure D.1. Influence of shaft speed on damped natural frequencies.

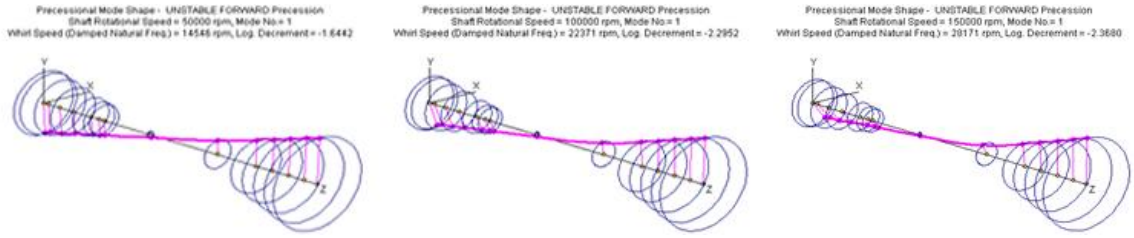

Figure D.2. FR 1st mode shapes with increased turbocharger shaft speed

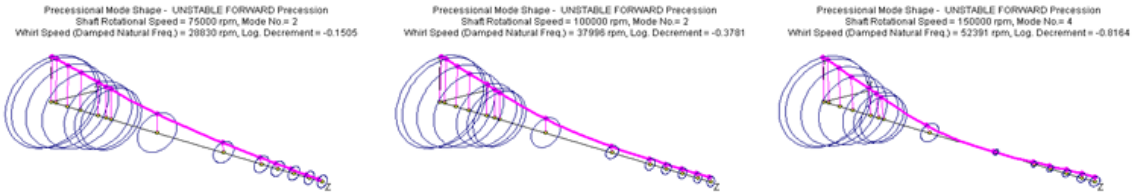

Figure D.3. FR 2nd mode shapes with increased turbocharger shaft speed

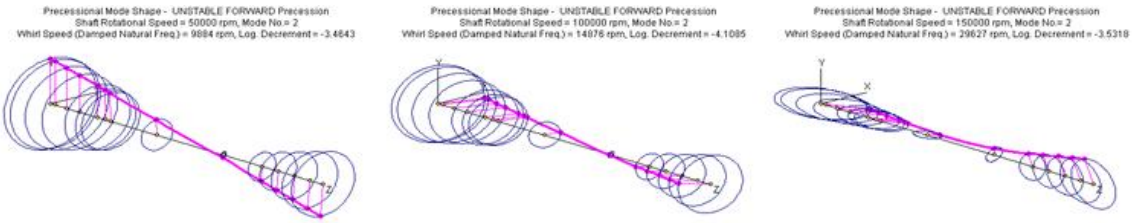

Figure D.4. 6AG 1st mode shapes with increased turbocharger shaft speed

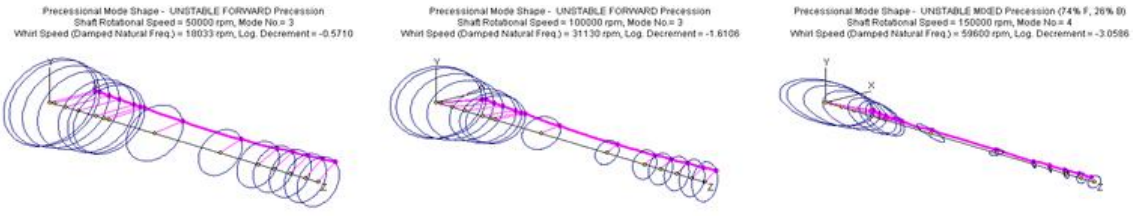

Figure D.5. 6AG 2nd mode shapes with increased turbocharger shaft speed

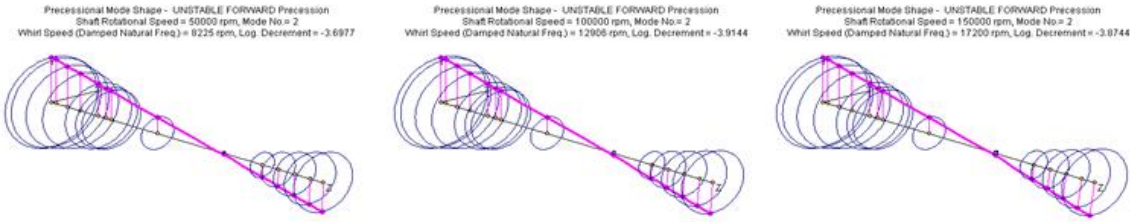

Figure D.6. 8AG 1st mode shapes with increased turbocharger shaft speed

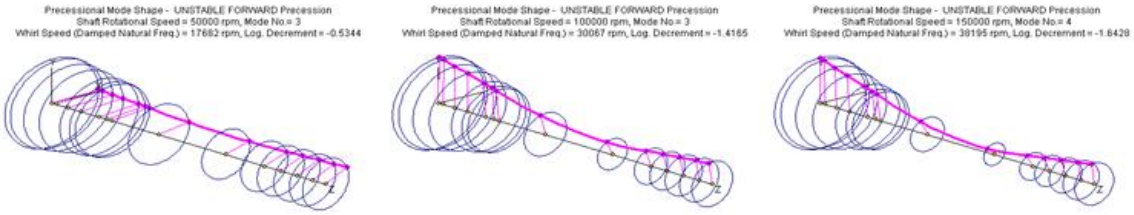

Figure D.7. 8AG 2nd mode shapes with increased turbocharger shaft speed

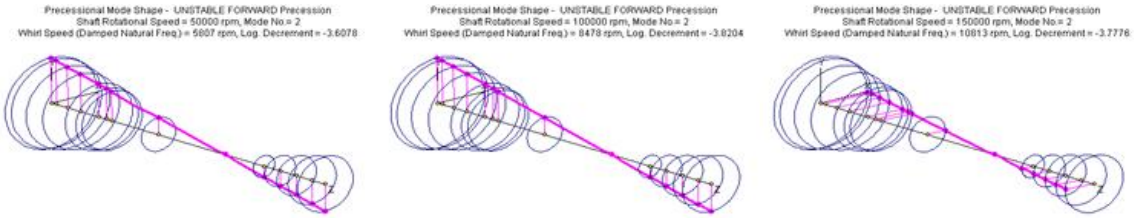

Figure D.8. 10AG 1st mode shapes with increased turbocharger shaft speed

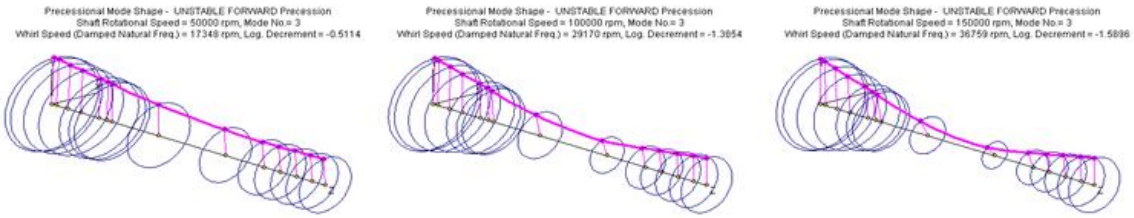

Figure D.9. 10AG 2nd mode shapes with increased turbocharger shaft speed

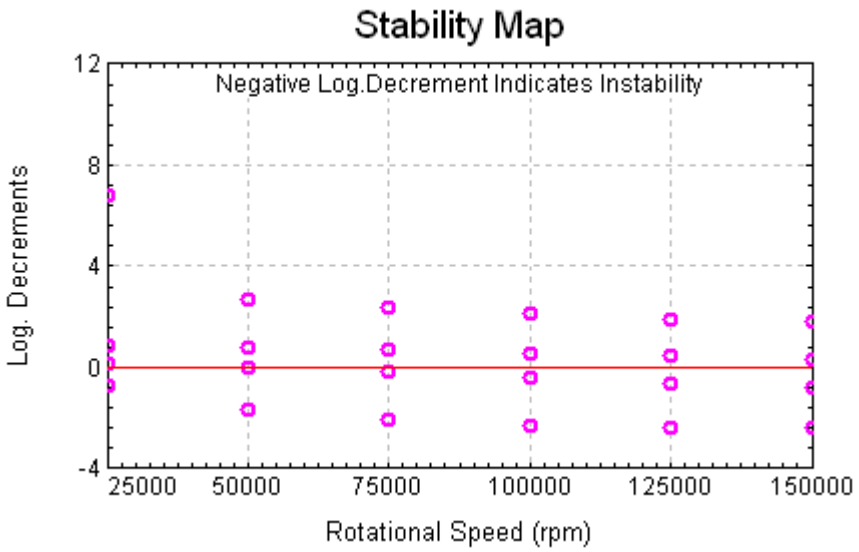

Figure D.10. Stability map for unloaded FR bearing

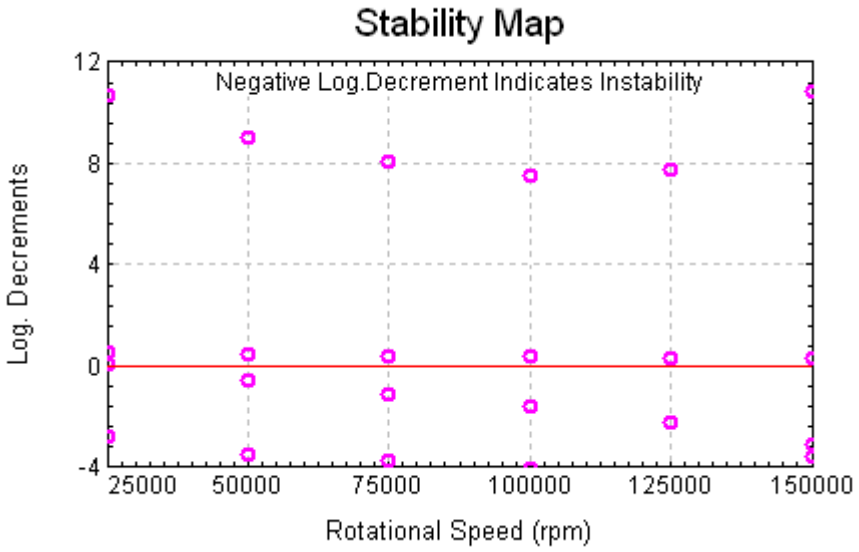

Figure D.11. Stability map for unloaded 6AG bearing

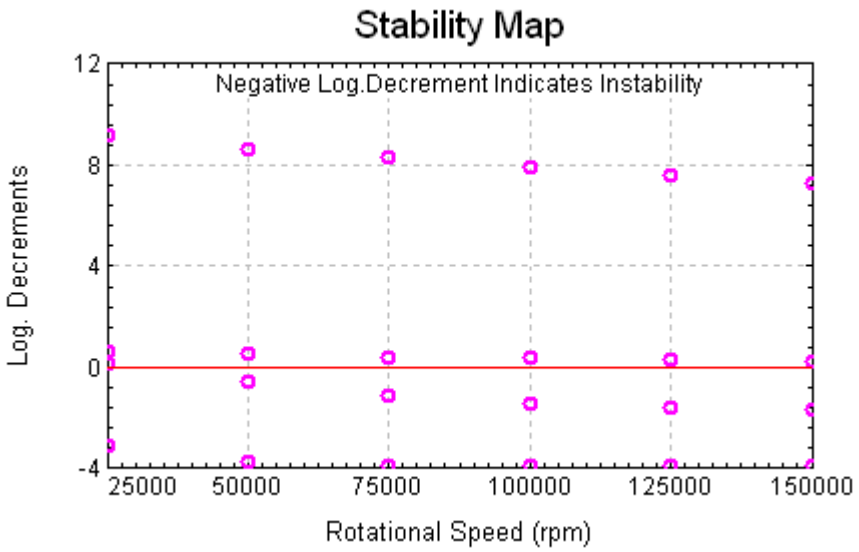

Figure D.12. Stability map for unloaded 8AG bearing

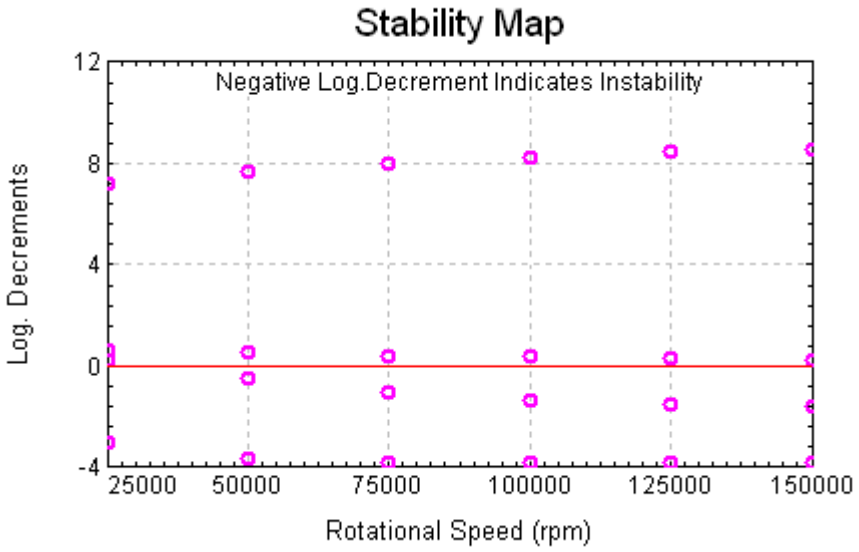

Figure D.13. Stability map for unloaded 10AG bearing

Appendix E

Influence of Axial Grooves on Damped Natural Frequency Data

Table E.1. Influence of axial grooves on damped natural frequencies

Red value in **bold** *italic* was a frequency that was previously unstable at gravity load.

Gravity Loads

	FR mode 1	FR 2	mode	6AG mode 1	6AG mode 2	8AG mode 1	8AG mode 2	10AG mode 1	10AG mode 2
25000	8691			6719		5503		4256	
50000	14546			9884	18033	8225	17682	5807	17348
75000	18875		28830	12478	25436	10642	24705	7199	24087
100000	22371		37966	14876	31130	12906	30067	8478	29170
125000	25419		45969	17420	35777	15081	34430	9676	33264
150000	28171		52391	19627	39600	17200	38195	10813	36759

5lb Load

	FR mode 1	FR 2	mode	6AG mode 1	6AG mode 2	8AG mode 1	8AG mode 2
25000	9908	na		10094	na	9537	na
50000	15199	na		13750	***21932***	12530	***21121***
75000	18815		26930	15968	28808	14843	27725
100000	21808		34432	17677	33367	16978	32639
125000	24750		40744	19380	37288	18477	36683
150000	27462		46232	20986	40631	20024	40057

10lb Load

	FR mode 1	FR 2	mode	6AG mode 1	6AG mode 2	8AG mode 1	8AG mode 2
25000	***11056***	na		***11241***	na	***10205***	na
50000	16588	na		15729	***25377***	14936	na
75000	19895		***28705***	18081	***32575***	17401	***32093***
100000	23196		36479	20260	36836	19363	35001
125000	25690		42396	21922	40104	20870	38900
150000	27947		47055	23387	42881	23384	43158

15lb Load

	FR mode 1	FR 2	mode	6AG mode 1	6AG mode 2	8AG mode 1	8AG mode 2
25000	***12020***	na		***11988***	na	***12398***	na
50000	17877	na		17118	***27326***	16790	na
75000	21203		***30365***	19828	***36497***	19253	***37232***
100000	24020		***38118***	21973	39794	21698	42070
125000	26662		44263	23765	42657	23336	41720
150000	28999		48869	25323	45163	24571	43957

Appendix F

Influence of Compressor Load on Damped Natural Frequency Data

Table F.1 FR mode 1 and 2 damped natural frequencies as a function of load

Red value in **bold** *italic* was a frequency that was previously unstable at gravity load.

FR	Mode 1					
	Unloaded	5lb	10lb	15lb	20lb	25lb
25000	8691	9908	***11056***	***12020***	***12923***	***13483***
50000	14546	15199	16588	17877	18822	19574
75000	18875	18815	19895	21203	22467	23231
100000	22371	21808	23196	24020	24999	25935
125000	25419	24750	25690	26662	27324	28059
150000	28171	27462	27947	28999	29701	30188
	Mode 2					
	Unloaded	5lb	10lb	15lb	20lb	25lb
25000						
50000						
75000	28830	26930	***28705***	***30365***	***31906***	***32970***
100000	37966	34432	36479	***38118***	***39765***	***39856***
125000	45969	40744	42396	44263	45583	47273
150000	52391	46232	47055	48869	49999	51316

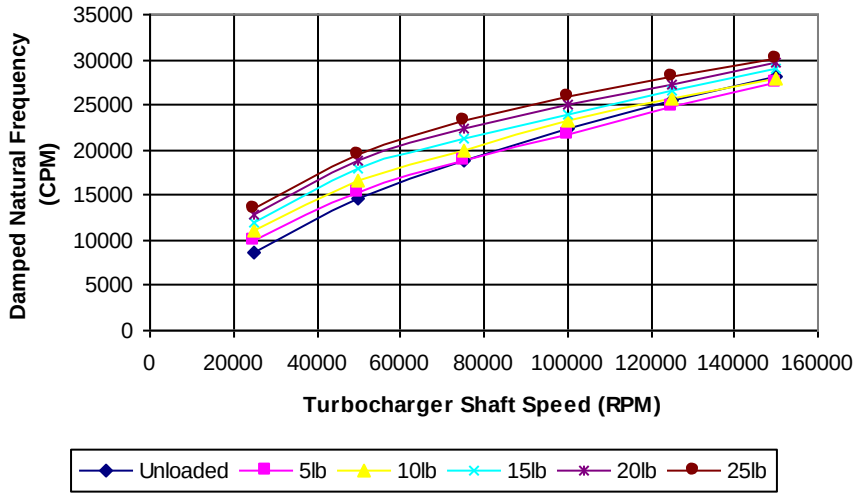

Figure F.1 FR 1st mode damped natural frequencies

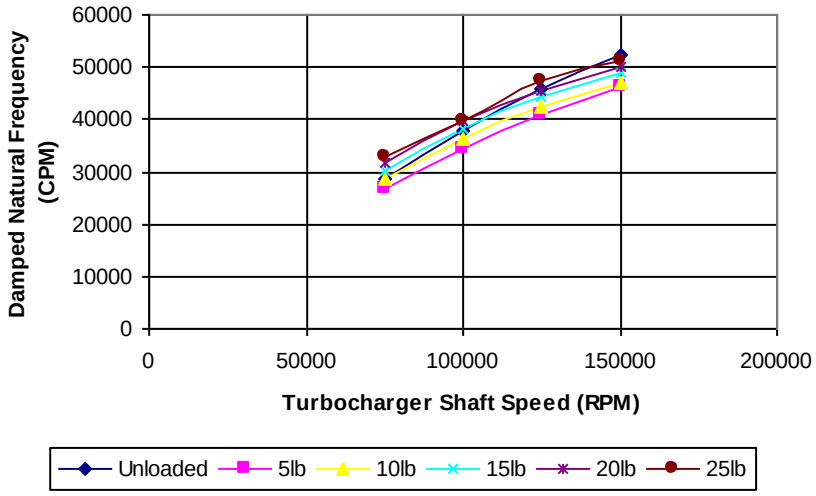

Figure F.2 FR 2nd mode damped natural frequencies

Table F.2 6AG 1st and 2nd mode damped natural frequencies as a function of load

Red value in **bold** *italic* was a frequency that was previously unstable at gravity load.

6AG	Mode 1					
	Unloaded	5lb	10lb	15lb	20lb	25lb
25000	6719	10094	***11241***	***11988***	***12260***	***12433***
50000	9884	13750	15729	17118	18035	18497
75000	12478	15968	18081	19828	21204	22101
100000	14876	17677	20260	21973	23253	24425
125000	17420	19380	21922	23765	25025	26147
150000	19627	20986	23387	25323	26637	27803
	Mode 2					
	Unloaded	5lb	10lb	15lb	20lb	25lb
25000						
50000	18033	***21932***	***25377***	***27326***		
75000	25436	28808	***32575***	***36497***	***38890***	***39737***
100000	31130	33367	36836	39794	42799	***45526***
125000	35777	37288	40104	42657	44759	46926
150000	39600	40631	42881	45163	46969	48841

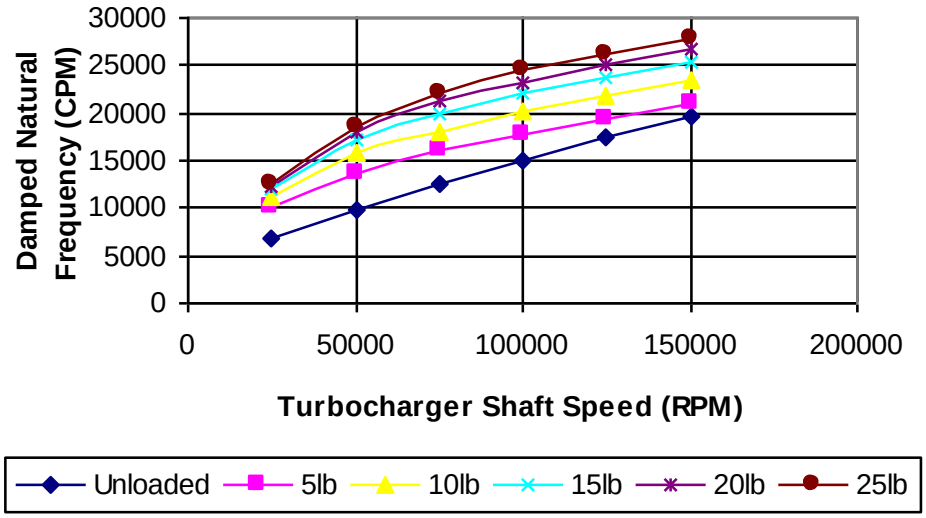

Figure F.3. 6AG 1st mode damped natural frequencies

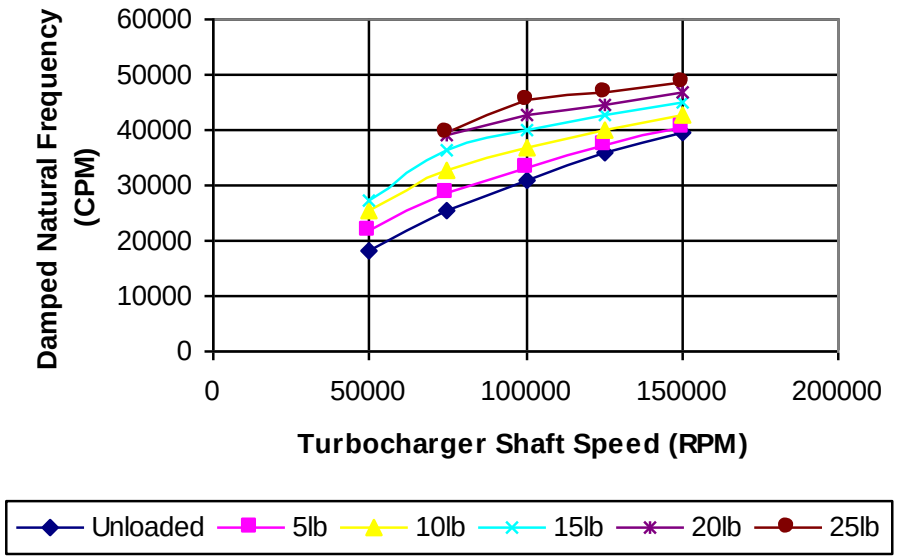

Figure F.4. 6AG 2nd mode damped natural frequencies

Table F.3 8AG 1st and 2nd mode damped natural frequencies as a function of load

Red value in **bold** *italic* was a frequency that was previously unstable at gravity load.

8AG	Mode 1			
	Unloaded	5lb	10lb	15lb
25000	5503	9537	***10205***	***12398***
50000	8225	12530	14936	16790
75000	10642	14843	17401	19253
100000	12906	16978	19363	21698
125000	15081	18477	20870	23336
150000	17200	20024	23384	24571
	Mode 2			
	Unloaded	5lb	10lb	15lb
25000				
50000	17682	***21121***		
75000	24705	27725	***32093***	***37232***
100000	30067	32639	35001	42070
125000	34430	36683	38900	42720
150000	38195	40057	43158	43957

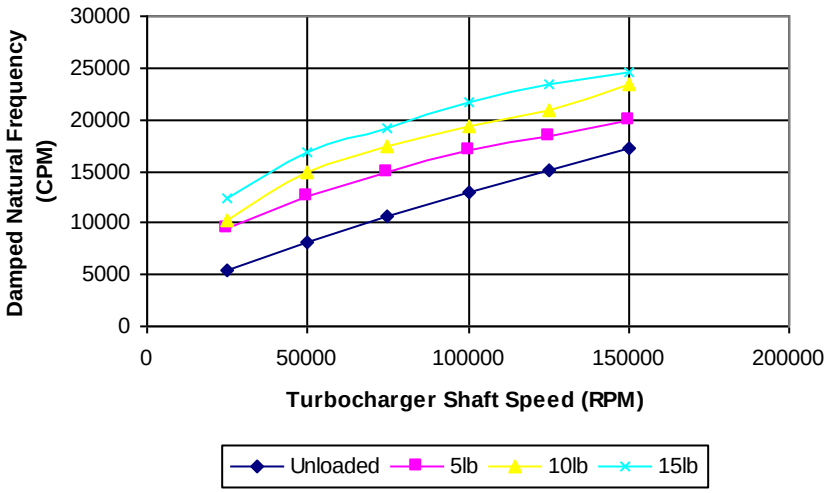

Figure F.5. 8AG 1st mode damped natural frequencies

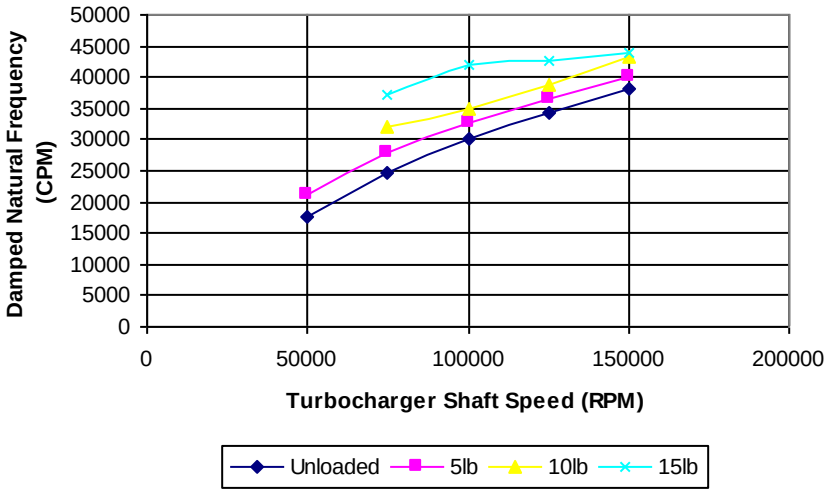

Figure F.6. 6AG 2nd mode damped natural frequencies

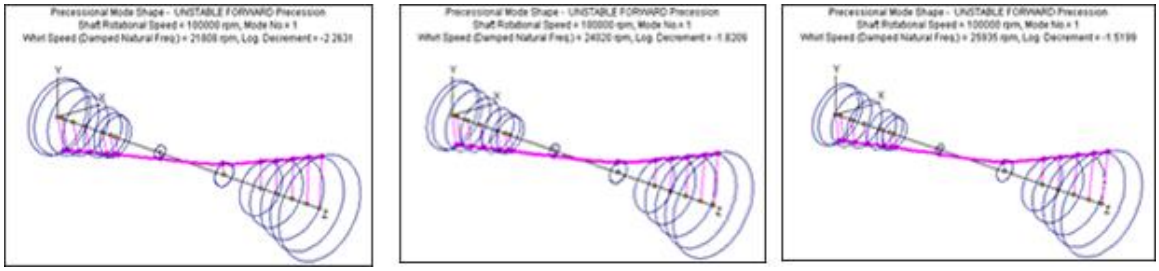

Figure F.7. FR 1st mode shape progression with increased loading

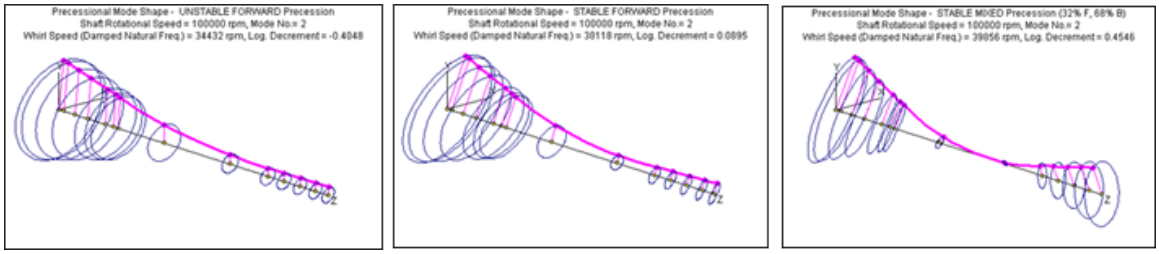

Figure F.8. FR 2nd mode shape progression with increased loading

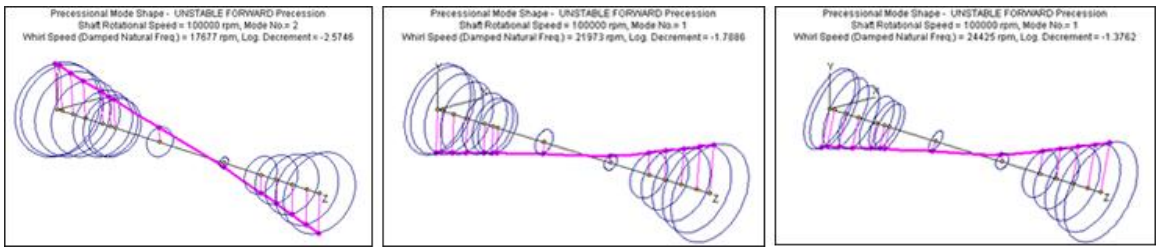

Figure F.9. 6AG 1st mode shape progression with increased loading

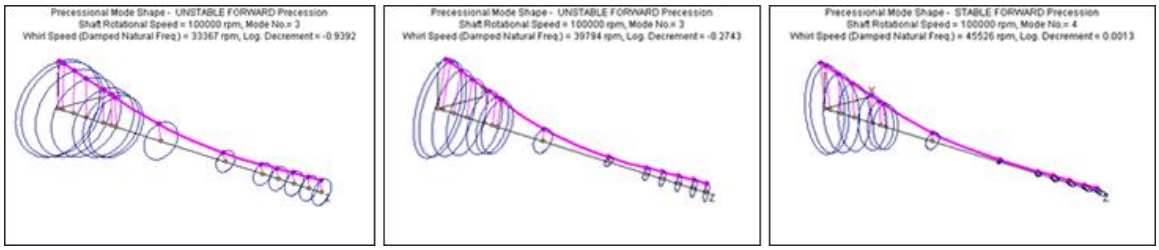

Figure F.10. 6AG 2nd mode shape progression with increased loading

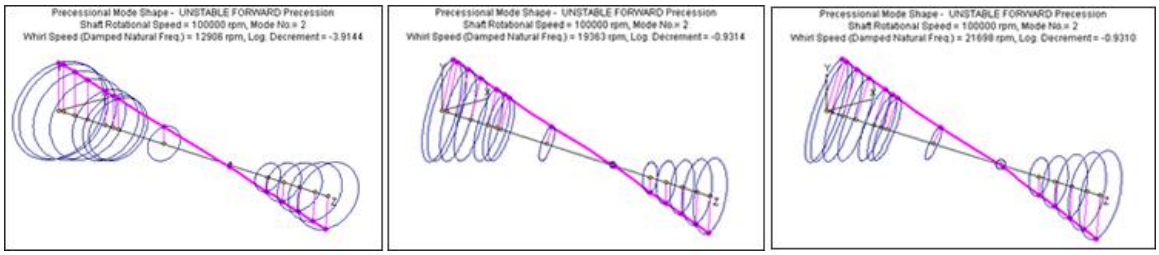

Figure F.11. 8AG 1st mode shape progression with increased loading

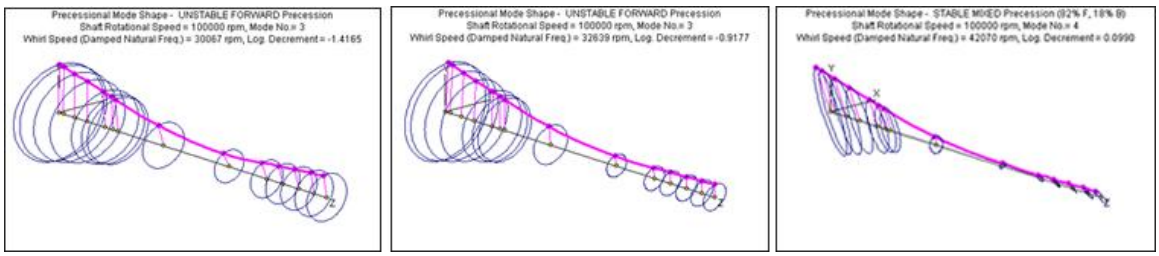

Figure F.12. 8AG 2nd mode shape progression with increased loading

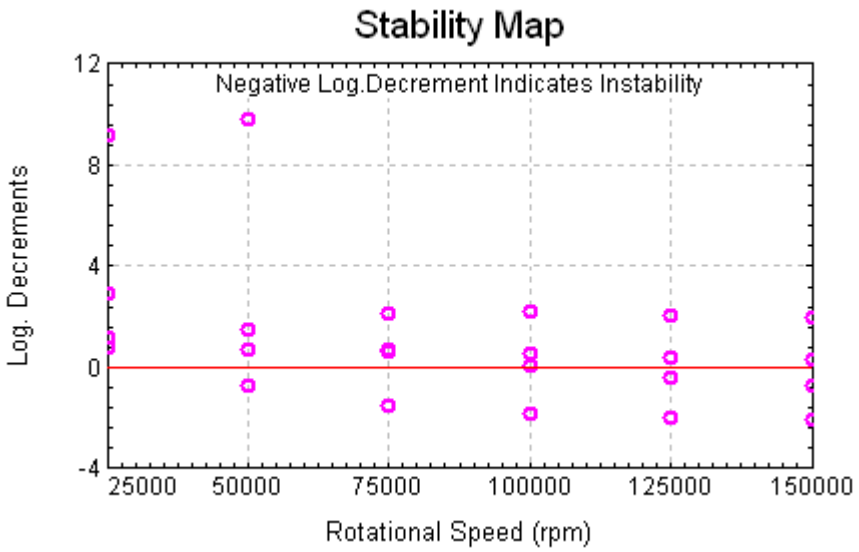

Figure F.13: Stability map for FR with 15lbs of compressor loading

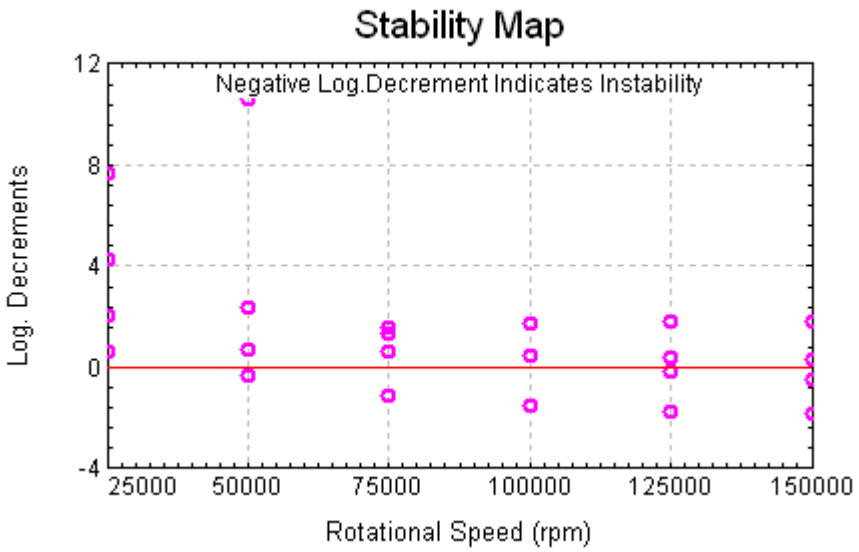

Figure F.14: Stability map for FR with 25lbs of compressor loading

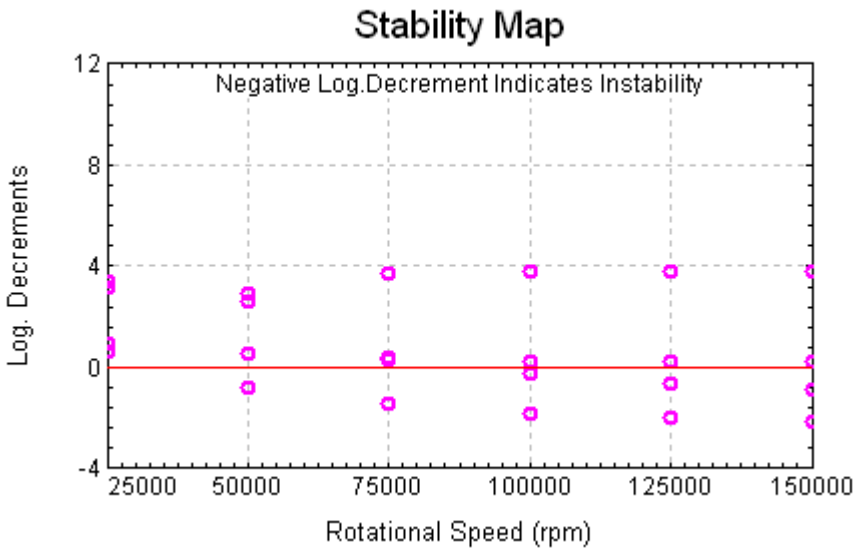

Figure F.15: Stability map for 6AG with 15lbs of compressor loading

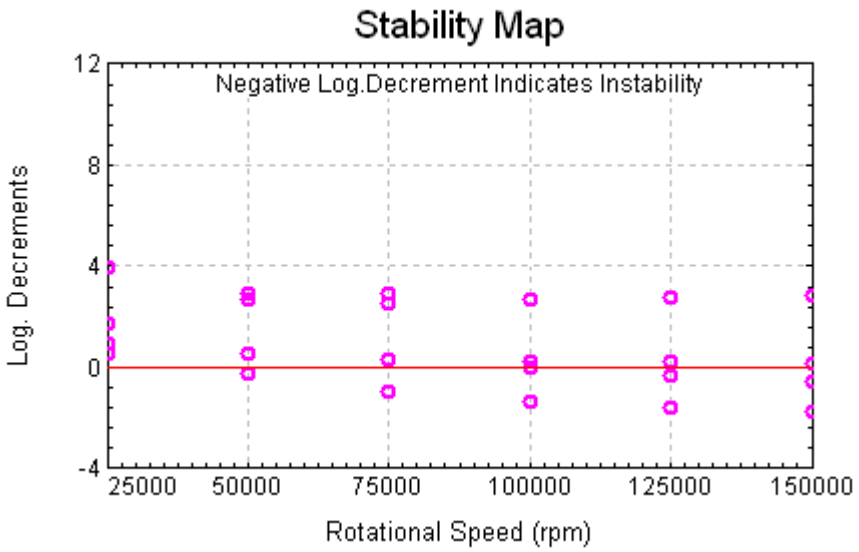

Figure F.16: Stability map for 6AG with 25lbs of compressor loading

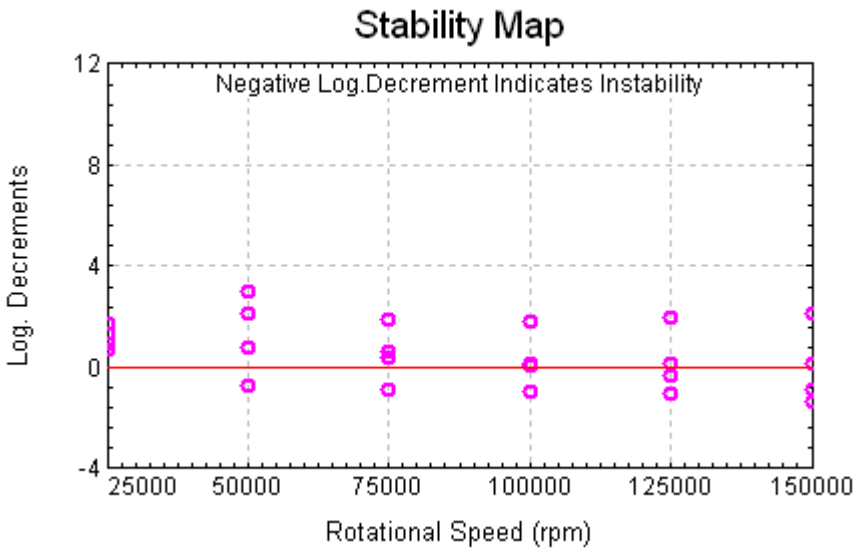

Figure F.17: Stability map for 8AG with 15lbs of compressor loading